Geomorphology 255 (2016) 63–80

Contents lists available at ScienceDirect

Geomorphology

journal homepage: www.elsevier.com/locate/geomorph

Hidden sinkholes and karst cavities in the travertine plateau of a highly-populated geothermal seismic territory (Tivoli, central Italy)

Andrea Billi [a,*], Luigi De Filippis [b], Pier Paolo Poncia [c], Pio Sella [d], Claudio Faccenna [a,c]

[a] Consiglio Nazionale delle Ricerche, IGAG, Rome, Italy
[b] Laboratorio R. Funiciello, Liceo L. Spallanzani, Tivoli, Rome, Italy
[c] Dipartimento di Scienze, Università Roma Tre, Rome, Italy
[d] Geomagellan, Monte Compatri, Rome, Italy

ARTICLE INFO

Article history:
Received 18 January 2015
Received in revised form 2 December 2015
Accepted 17 December 2015
Available online 19 December 2015

Keywords:
Sinkhole
Travertine
Natural hazard
Anthropogenic landform
Human–environment interaction
Anthropocene morphology

ABSTRACT

Sinkholes and other karst structures in settled carbonate lands can be a significant source of hazard for humans and human works. Acque Albule, the study area of this work, is a Plio-Pleistocene basin near Rome, central Italy, superficially filled by a large and thick deposit of late Pleistocene thermogene travertine. Human activities blanket large portions of the flat territory covering most evidence from geological surface processes and potentially inducing scientists and public officials to underestimate some natural hazards including those connected with sinkholes. To contribute to the proper assessment of these hazards, a geomorphologic study of the basin was performed using digital elevation models (DEMs), recent aerial photographs, and field surveys. Historical material such as old aerial photographs and past geomorphologic studies both pre-dating the most part of quarrying and village building was also used together with memories of the elderly population. This preliminary study pointed out the presence of numerous potentially active sinkholes that are at present largely masked by either quarrying or overbuilding. Where this first study pointed out the apparent absence of sinkholes in areas characterized by high density of buildings, a detailed subsurface study was performed using properly-calibrated electrical resistivity tomography (ERT) and dynamic penetration measurements (DPSH), together with some borehole logs made available from the local municipality. This second study highlighted the presence of sinkholes and caves that are, this time, substantially hidden to the resolution of standard methods and materials such as aerial photographs, DEMs, and field surveys. Active sinkhole subsidence in the Acque Albule Basin may explain, at least in part, the frequent damages that affect numerous buildings in the area. The main conclusion from this study is that the mitigation of sinkhole hazard in highly populated areas has to pass through a thorough search of (hidden) sinkholes that can be masked by the Anthropocenic molding and blanketing of the territory. For these purposes, data from historical (pre-Anthropocene) documents as well as, where possible, subsurface investigations are fundamental.

1. Introduction

Sinkholes (or dolines) are depressions or holes in the ground generated by some form of slow subsidence or sudden collapse induced by physical–chemical erosion of rocks in the shallow subsurface (Fig. 1). Most sinkholes are caused by carbonate karst processes (i.e., chemical dissolution of carbonate rocks), but these structures can similarly form also in other rocks and minerals such as salt and gypsum. Sinkholes may vary in size from a few to hundreds of meters both in diameter and depth, and, as mentioned above, may form gradually or, more often, through a sudden collapse. The formation of these latter sinkholes can be dramatic, as the surface land usually stays intact until there is not enough support. At this time, a sudden collapse of the land surface can occur with possible dramatic consequences for humans, buildings, and infrastructures (Jennings, 1985; Gillieson, 1987; Ford and Williams, 1989; Faccenna et al., 1993; Salvati and Sasowsky, 2002; van Schoor, 2002; Waltham and Fookes, 2003; Williams, 2004; Beck, 2005; Waltham et al., 2005; Yechieli et al., 2006; Ford, 2006; Gutiérrez et al., 2007, 2009, 2014; Bruno et al., 2008; Faulkner, 2009; Valois et al., 2011; Brinkmann, 2013; Ezersky and Frumkin, 2013; Gulley et al., 2013; Siart et al., 2013; Carbonel et al., 2014a; Simón et al., 2014; Poppe et al., 2015). Hence, populated sinkhole-prone areas necessitate specific prevention and management measures (Sowers, 1996; Ford, 2006; Epting et al., 2009; Hao et al., 2009; Song et al., 2012; Siart et al., 2013; Carbonel et al., 2014a,b; Gill and Malamud, 2014).

In central Italy, which is the carbonate sinkhole-prone study area of this paper (Fig. 2), sudden occurrences of sinkholes have happened on several occasions in recent and historical times (Faccenna et al., 1993;

* Corresponding author at: CNR-IGAG at Dipartimento di Scienze della Terra, Università Sapienza, Piazzale A. Moro 5, Rome 00185, Italy.
E-mail address: andrea.billi@cnr.it (A. Billi).

http://dx.doi.org/10.1016/j.geomorph.2015.12.011
0169-555X/© 2015 Published by Elsevier B.V.

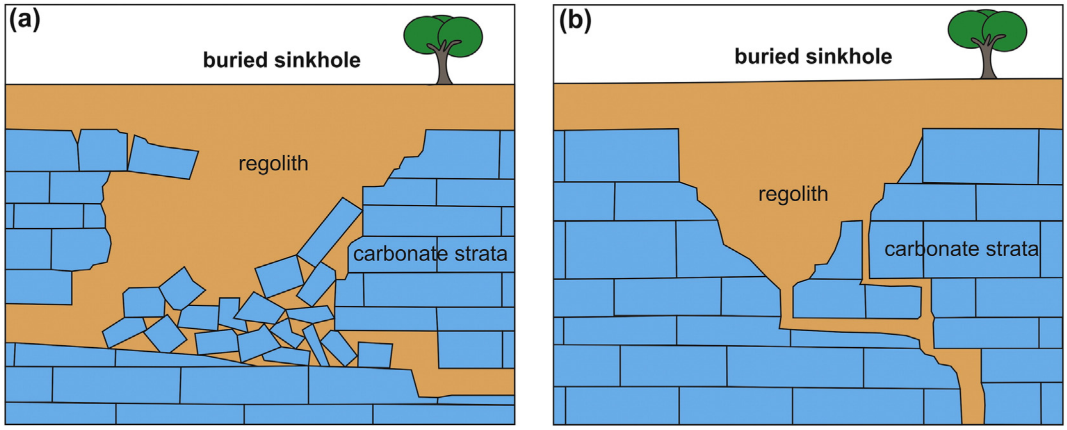

Fig. 1. Conceptual sketches of two types of buried (hidden) sinkholes (modified from and inspired by Ford and Williams, 1989, Gunn, 2004, Waltham et al., 2005, and Nisio et al., 2007). These types of sinkholes are common in the travertine substratum of the Acque Albule Basin and visible along the travertine quarry walls (Figs. 2–5). (a) Buried (hidden) cave-collapse sinkhole filled by soil and regolith after (and partly before) the collapse of the carbonate vault. (b) Buried (hidden) solution sinkhole (also commonly known as doline) filled by soil and regolith after the chemical (and partly physical) erosion of the carbonate substratum. Both sinkholes in (a) and (b) are drawn as apparently inactive (i.e., no surface depression).

Salvati and Sasowsky, 2002; Nisio et al., 2007; Nisio, 2008; Caramanna et al., 2008; Centamore et al., 2009; Guarino and Nisio, 2012; Amanti and Nisio, 2013; Billi et al., 2014; Ciotoli et al., in press). Sinkholes, however, are dangerous and harmful for humans and human works not only when the collapse abruptly occurs, but also after the collapse when they are totally filled, apparently extinct, and de facto hidden (Fig. 1). The filling, in fact, can be made of unconsolidated soft clay-to-sand allogenic deposits and soil (regolith) that may easily be compacted and depressed under the load of a construction or may be the locus of a new sudden collapse through the slow process of suffosion or, more in general, through sinkhole rejuvenation processes (i.e., cover-collapse sinkhole and cover-subsidence sinkhole; Waltham et al., 2005; Ford, 2006; Koutepov, 2008; Zhou and Beck, 2008; Billi et al., 2014). Suffosion, in particular, occurs when loose soil or other non-cohesive material that lies on top of a karst-carved limestone substratum containing fissures and joints is gradually washed downward through the fissures and into the caves beneath, thus creating a depression on the landscape of varying depth and diameter.

All the above-mentioned phenomena leading to sinkhole formation can be highly favored by geothermal and seismic processes leading to, for instance, pressurized geothermal circulation or seismic shaking (Heidari et al., 2011; Santo et al., 2011; Sella et al., 2014). The case of slow compaction and subsidence on top of sinkholes filled by ground and regolith under the load of multi-story buildings in a geothermal-seismic area seems to be the case of the densely-populated and (in places) overbuilt Acque Albule Basin, Tivoli, central Italy (Fig. 2). This is a Plio-Pleistocene basin near Rome, partly filled by a late Pleistocene travertine large deposit that is a few tens of meters thick and on the order of 1 km^3 in volume (Maxia, 1950; Faccenna et al., 1994, 2008; De Filippis et al., 2013a,b). The travertine originated by the subsurface circulation through the Meso-Cenozoic marine carbonates of groundwater enriched in CO_2 and other endogenic elements by the nearby quiescent and degassing Colli Albani volcano (Manfra et al., 1976; Minissale et al., 2002; Vignaroli et al., 2015). The geothermal circulation is still active and inverse erosion (bottom-up) is one of the causes of carbonate chemical dissolution

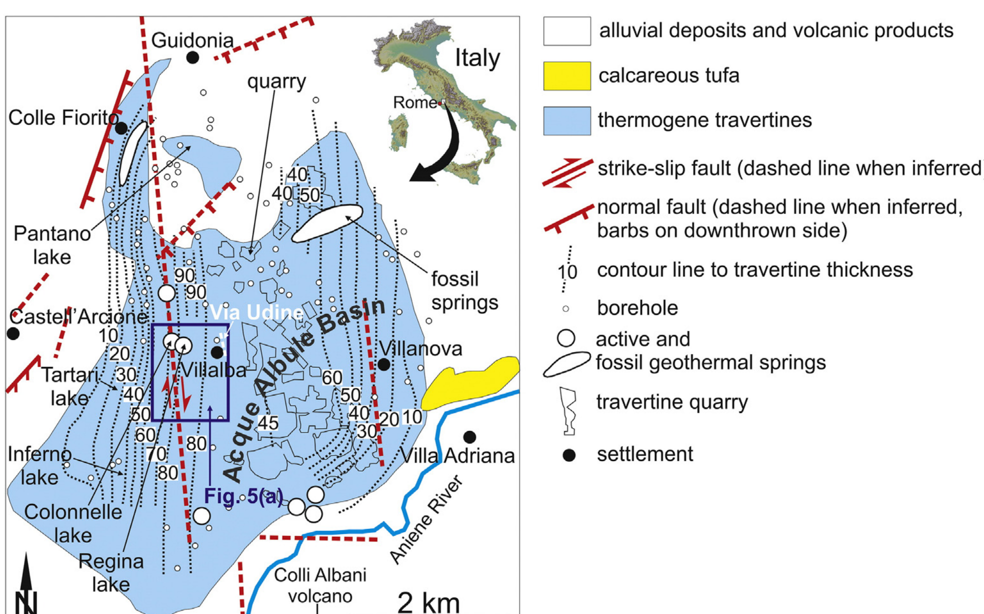

Fig. 2. Geological setting of the geothermally- and seismically-active Acque Albule Basin close to Rome (c. 25 km distant), central Italy. In its upper section, the basin is largely filled by a late Pleistocene thick (maximum thickness: c. 90 m) thermogene travertine deposit (Faccenna et al., 2008), which is rich in various karst features and sinkholes (Figs. 3–5).

and sinkhole formation (Billi et al., 2007; see also Frumkin et al., 2015).

The Tivoli travertine deposit is known from large exposures in huge active quarries (Fig. 3) and inferred in the shallow subsurface from boreholes and geophysical data in the area surrounding the quarries (Faccenna et al., 2008). In the quarry exposures as well as over the topographic surface, filled sinkholes and other karstic structures are clearly visible (Figs. 3, 4, 5b–d) and constitute an important comparison term to correctly interpret the borehole and subsurface geophysical data where the travertine is not exposed. In the basin, in effect, where the travertine body is not quarried and appears as mostly covered by soil, regolith, and cement, some recent buildings are slowly sinking and are affected by fractures and other damages (Brunetti et al., 2013; De Filippis et al., 2013c; Floris et al., 2014; Bozzano et al., 2015). The study of pre-construction aerial photographs (taken in 1943) revealed that some of these edifices were built right on top of void sinkholes

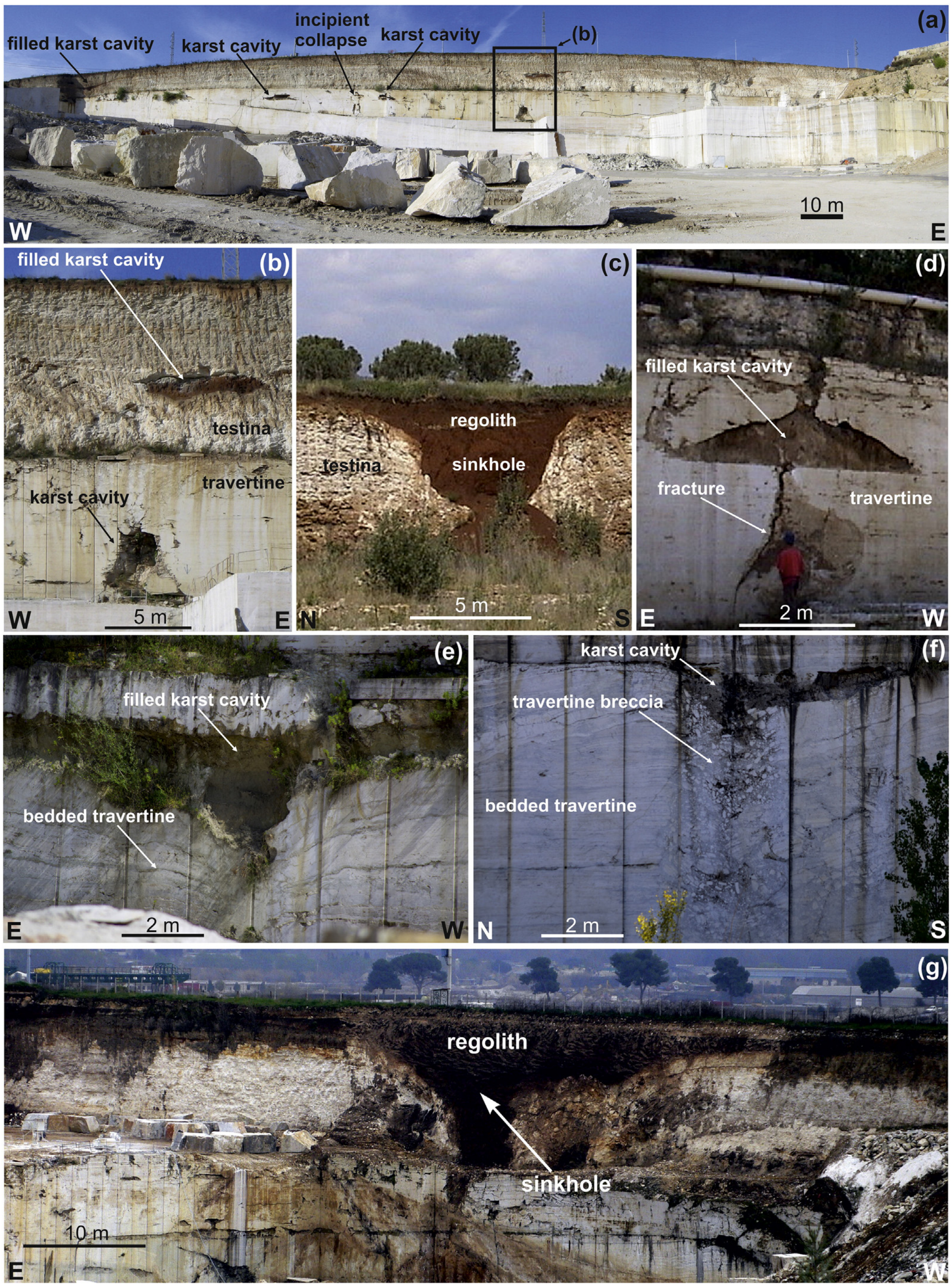

Fig. 3. Photographs of travertine exposures and related karst structures in the Acque Albule Basin quarries. (a) Panoramic view of a travertine quarry. (b) Enlargement from the previous photograph. The travertine succession is characterized by a compact poorly- to non-porous thick travertine deposit that is usually overlain by a very porous poorly-cemented travertine named "testina" that is up to a few meters thick. The testina travertine is usually overlain by regolith and soil for a thickness between a few centimeters and a few meters or even more depending upon the presence of karst structures. (c) Filled sinkhole within the testina travertine. (d) Filled karst cavity (future potential sinkhole) within the compact travertine lying below the testina. (e) Karst cavity filled by allogenic deposits within the compact travertine. (f) Karst cavity filled by allogenic deposits and travertine breccia within the compact travertine. (g) Large solution sinkhole filled by soil and regolith in the shallow portion of the travertine deposit. We used this quarry wall exposure as the calibration site for the acquisition of ERT and penetration data (DPSH) as explained in the text and in the following figures.

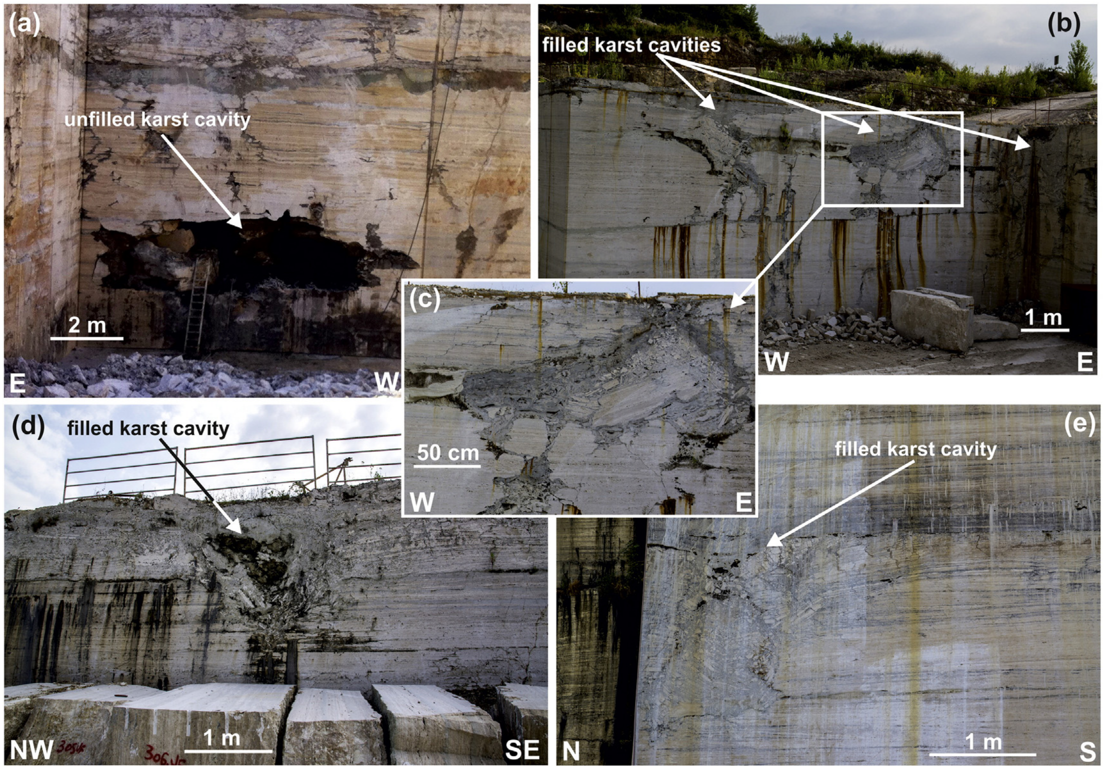

Fig. 4. Further photographs of travertine exposures and related karst structures in the Acque Albule Basin quarries. These photographs and those of Fig. 3 are useful to interpret the subsurface data presented in the next figures. (a) Large unfilled karst cavity. (b) Karst cavities filled by travertine clasts and blocks (breccia) and by travertine cement. (c) Enlargement from the previous photograph showing the travertine filling within a karst cavity. (d) and (e) Karst cavities filled by travertine clasts and blocks (breccia) and by travertine cement.

(compare Fig. 5a vs. b and c vs. d), which must have therefore been artificially filled before the edifice construction. In the same area, however, there are numerous other buildings that are sinking or have sunk for apparently no reason, suggesting the presence of hidden sinkholes or similar karst structures in the shallow subsurface that may be dangerous for human surface activities (Brunetti et al., 2013; Billi et al., 2013; De Filippis et al., 2013c; Floris et al., 2014; Bozzano et al., 2015). Moreover, the Acque Albule Basin and the nearby Apennines fold–thrust belt are seismically-active areas (Gasparini et al., 2002; Chiarabba et al., 2009; for the corresponding seismic classification the reader is referred to http://zonesismiche.mi.ingv.it/). Seismic shaking may have favored in the past, and may favor in the future, both the sudden collapse of sinkholes and the gradual subsidence of sinkhole-filling-ground. Similarly, the pressurized aggressive geothermal circulation of the Acque Albule Basin may enhance karst dissolution and suffosion processes (e.g., Billi et al., 2007, 2014; Caramanna et al., 2008; Santo et al., 2011; Ciotoli et al., 2013; Pirro et al., 2013; Sella et al., 2014; Bigi et al., 2014).

For the above-reported reasons, the Acque Albule Basin in the Tivoli area (Fig. 2) is an excellent case history where searching, discovering, and studying hidden sinkholes or similar karst structures in the shallow subsurface of a densely populated surface and learning how to manage or at least assess this environmental source of hazard (e.g., Zhou and Beck, 2008; Carbonel et al., 2014b). Our main aim, in particular, is to understand whether standard aerial photographic studies together with digital elevation model (DEM) analyses and field surveys can be sufficient to constrain the presence of buried (hidden) sinkholes and caves (i.e., future potential sinkholes) or whether further analyses are necessary. To do so, firstly, we have performed a general geomorphologic study of the Acque Albule Basin using standard methods and materials such as aerial photographs, DEMs, and field surveys. We have integrated this material with historical pre-quarrying and pre-building documents. This first study has highlighted the presence of numerous visible or recently-visible sinkholes. Secondly, where our first study pointed out an apparent absence of sinkholes in areas characterized by high density of buildings, we have performed a detailed subsurface study using properly-calibrated electric resistivity tomography (ERT) and penetration methods (DPSH) as well as borehole logs from nearby areas. Also this second study has highlighted the presence of sinkholes and caves that are, this time, substantially hidden to the resolution of standard methods and materials. We believe that our results can be useful in understanding how to manage and assess the environment in overbuilt, highly-populated, sinkhole-prone, geothermal-seismic areas such as the Acque Albule Basin and elsewhere (e.g., Zhou and Beck, 2008; Harley et al., 2011; Carbonel et al., 2014a,b).

2. Geological setting

The Acque Albule Basin is located in the western (Tyrrhenian) portion of the central Apennines fold–thrust belt (Italy), which grew with an eastward piggy-back sequence of thrust sheets during late Miocene–Pliocene time. The western portion of this belt has undergone post-orogenic extensional tectonics since about Messinian–Pliocene time onward connected with the opening, toward the west, of the Tyrrhenian back-arc basin (Patacca et al., 1992; Cavinato and DeCelles, 1999; Billi et al., 2006; Billi and Tiberti, 2009). This extensional regime caused the formation of numerous Pliocene–Quaternary sedimentary basins and magmatic districts all along the Tyrrhenian–Apennines margin (e.g., Acocella and Funiciello, 2006; Rossetti et al., 2007). One of these districts includes the quiescent Colli Albani volcano and the adjacent peri-volcanic hydrothermal area of the Acque Albule Basin (Faccenna et al., 2008; Vignaroli et al., 2015).

The Acque Albule flat area hosts a sedimentary basin of Plio-Pleistocene age (Fig. 2). The basin is circa 30 km^2 in horizontal areal extension, circa 60 m in altitude a.s.l., and it is filled, in its upper section, by a large and thick travertine body of late Pleistocene age and thermogene origin (Figs. 3, 4). As we will show in the following, this deposit is rich in various karst features and sinkholes (Figs. 4, 5; Salvati and Sasowsky, 2002; Billi et al., 2007; Caramanna et al., 2008; Faccenna et al., 2008;

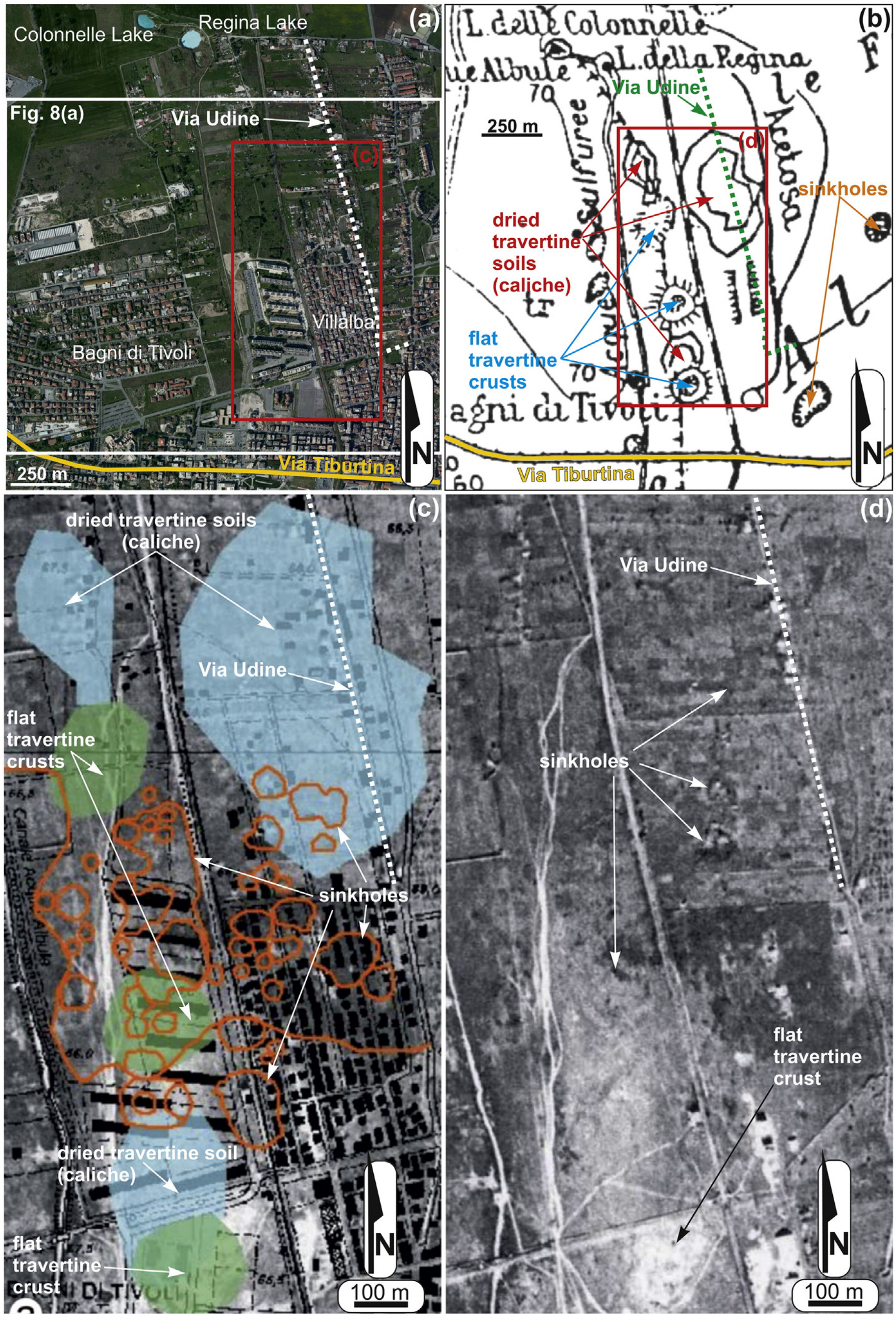

Fig. 5. (a) Aerial photograph (from Bing Maps) of the Villalba village area in the Acque Albule Basin (see location in Fig. 2). (b) Excerpt from the geomorphologic map of Maxia (1950), showing a series of circular depressions (sinkholes) and other geomorphologic structures in the Villalba area before the edification of the village, which has mostly grown since about 1960s. Note that the areas shown in panels (a) and (b) are roughly the same. (c) Geomorphic map of the Villalba area (excerpt from Fig. 7). See location of this image in panel (a). (d) Aerial photograph of the Villalba area taken by the RAF (Royal Air Force) in 1943 before the construction of the village. Note the presence of void holes (sinkholes) over the land where edifices presently occur (see panel c). Note that the areas shown in panels (c) and (d) are roughly the same.

Argentieri et al., 2015). The subsurface thickness of the travertine, which is flat to gently-dipping with no topographic prominences except for the Colle Fiorito ridge (see Fig. 2; De Filippis et al., 2013a), is on average circa 50 m and up to about 90 m at its maximum coinciding with one or more seismically-active faults lying beneath the travertine deposit. This deposit lies over a sequence of marine and continental clays, sands, and conglomerates of Plio-Pleistocene age alternated, in the upper portion, with Pleistocene volcanic products deriving from the nearby active or recently-active (quiescent) Colli Albani and Sabatini volcanic districts. The travertine deposit, which is very compact and strong, is usually covered by a few meters of a poorly-cohesive and poorly-diagenized travertine, locally named testina (Fig. 3a–b). The testina, in turn, is covered by the regolith and recent-to-present soil that can be a few decimeters to a few meters thick (Fig. 3c, g; Maxia, 1950; Faccenna et al., 1994, 2008; Gasparini et al., 2002; De Filippis et al., 2013a,b).

The Acque Albule Basin and nearby areas are characterized by intense karst processes with formation of numerous structures including sinkholes and caves (Figs. 3, 4, 5). Some of these structures are clearly visible on the surface (Fig. 5) and host, in some instances, geothermal springs and lakes (e.g., Colonnelle and Regina lakes; Fig. 2) or dried lakes presently filled by continental deposits (e.g., Tartari and Pantano lakes; Fig. 2) (Billi et al., 2007; Nisio et al., 2007; Nisio, 2008; Caramanna et al., 2008; Centamore et al., 2009; Guarino and Nisio, 2012; Amanti and Nisio, 2013; Argentieri et al., 2015). The basin subsidence, hydrothermal circuit and, consequently, travertine formation have been controlled by the presence and activity of faults beneath and along the boundaries of the basin. The main faults are N–S-striking with a right-lateral strike-slip to transtensional kinematics. Other associated faults are NE-striking with an oblique to normal kinematics. The main N–S-striking strike-slip fault is documented on outcrops of the Lucretili Mts. immediately to the north of the basin, whereas the fault southward prolongation beneath the basin coincides with the two main thermal springs (i.e., Colonnelle and Regina lakes; Fig. 2) (Maiorani et al., 1992; Faccenna et al., 1994, 2008; Billi et al., 2007; De Filippis et al., 2013a,b).

The Acque Albule Basin is a low seismicity area (Gasparini et al., 2002; Frepoli et al., 2010). In 2001–2002, in particular, a long-lasting seismic sequence was recorded using the national seismic network and an additional local temporary one. Results showed that the shallow earthquake hypocenters (2 km deep at the most) were aligned along one of the known faults in the basin (Gasparini et al., 2002). Moreover, it is important to mention that the pressurized local geothermal circuit can be influenced by intermediate and strong (4–6 M_w classes) earthquakes usually occurring in nearby regions (i.e., central Apennines and Colli Albani volcano; Frepoli et al., 2010). For instance, the seismic waves generated by the 2009 L'Aquila earthquake (M_w 6.3; Chiarabba et al., 2009) provoked piezometric variations in the Acque Albule Basin, probably connected with transient changes of permeability (La Vigna et al., 2012, 2013a; see also Plastino et al., 2010, 2011). Moreover, in the same occasion, a remarkable transient increase of degassing (mostly CO_2 accompanied by minor H_2S) from the Acque Albule geothermal springs (in particular, from the Colonnelle and Regina lakes) was observed. Due to the gas hazard, the area of the geothermal springs was strictly forbidden to people for a period of a few days after the 2009 L'Aquila earthquake, whose epicentral area is located c. 70 km to the northeast of the Acque Albule Basin.

The hydrogeological and geothermal regime of the Acque Albule Basin is dominated by the large carbonate recharge area (Apennines Mts.) to the north, northeast, and east of the basin (i.e., the Apennines fold–thrust belt) and by the presence of N- to NE-striking faults and damage zones (Billi et al., 2007; e.g. Billi and Salvini, 2000) that carry a large amount of groundwater (partly heated by the nearby quiescent volcanic districts) toward the basin, where the water discharge is huge, around 5 m^3/s. The groundwater mainly travels in carbonate karst aquifers and, approaching the Acque Albule Basin, is enriched in the subsurface by CO_2, S, and other gases and volatile elements deriving from the degassing processes active all around the adjacent hydrothermally-active Colli Albani volcano. These geothermal waters are characterized by a low thermality (c. 22.5 °C) and are rich in CO_2, H_2S, Fe, and other elements (Capelli et al., 1987; Carucci et al., 2012; Brunetti et al., 2013; Di Salvo et al., 2013; La Vigna et al., 2013b). The groundwater chemical content from the Regina Lake (see Fig. 2 for location) is presented in Table 1 (La Vigna et al., 2012).

The hydrogeology of the Acque Albule Basin is characterized by two main hydraulically-connected aquifers: the deep one is thermal and partly confined into the km-thick carbonate bedrock of Meso-Cenozoic age, whereas the shallow one is unconfined in the Pleistocene travertine. The two aquifers are separated by a non-continuous clayey aquiclude (La Vigna et al., 2013a). The shallow aquifer is, at present, strongly dewatered by travertine quarry activities (Brunetti et al., 2013; Floris et al., 2014; Bozzano et al., 2015; Del Bon et al., 2015).

3. Geomorphologic map of the Acque Albule Basin

3.1. Workflow and method

We started our work on hidden sinkholes and other karst structures of the Acque Albule Basin by compiling a general geomorphologic map of this area. To study the main geomorphologic features, we used a digital elevation model at a horizontal resolution of 20 × 20 m and a maximum vertical resolution of 5 m created after the digitalization of contour lines and elevation points from topographic maps at the 1:25,000 scale provided by IGMI (Istituto Geografico Militare Italiano; Fig. 6). We then used different sets of aerial photographs and images including the 1943 RAF (Royal Air Force survey, July–November 1943; Fig. 5d) set, the IGMI (1984–1985) set, and two most recent sets derived from satellite imagery of Google Maps and Bing Maps. The set from IGMI was, in particular, analyzed under stereoscopic view. To map and study the geomorphologic features evident prior than the largest part of quarrying and edifice building occurred, we used the 1943 RAF set of aerial photographs (e.g., Fig. 5d) and the results from the geologic–geomorphologic work realized by Maxia (1950); e.g. Fig. 5b). Moreover, where possible, we interviewed local elderly inhabitants who provided important information about pre-setting geomorphology of the surrounding countryside and about past natural phenomena such as terrain collapses and depressions, earthquakes, and hydrological regime changes. These memories, together with the collected historical material, allowed us to generate a geomorphologic map of the study area (Fig. 7), despite its present massive overbuilding and quarrying. Finally, we have corroborated and integrated the remote geomorphologic study with field surveys and in situ geomorphic mapping at various scales (around 1:5000 or larger) depending on the situations.

3.2. Results

The Acque Albule Basin is characterized by a generally flat to gently-dipping morphology (Fig. 6) that roughly coincides with the top surface of the southward-prograding travertine deposit (Faccenna et al., 2008) with its covering regolith and present soil. The western portion is characterized by altitudes between about 30 and 100 m a.s.l. and slope gradients lower than about 4% generally toward the south and south-east. The eastern portion is characterized by altitudes between about 30 and 80 m a.s.l. and slope gradients lower than about 2% toward the south and south-east. As mentioned above, this slope gradient roughly coincides with that of the underlying travertine clinostratification (Faccenna et al., 2008). The only morphological prominence in the study area is, toward the north-west, the N–S-oriented Colle Fiorito ridge (Figs. 6, 7), which was studied previously and interpreted as a travertine fissure ridge grown on top of the sequence of marine and continental deposits of Plio-Pleistocene age, aside the main travertine body that fills the Acque Albule Basin toward the east (De Filippis et al., 2013a).

The surface hydrographic network is poorly developed, probably for the presence of a well-developed sub-surface karst network in the Pleistocene travertine deposit (Figs. 3, 4) and in the underlying Meso-Cenozoic thick carbonate succession (Capelli et al., 1987). Toward the south, the Aniene River is the major hydrographic feature in the area and, with its length of c. 100 km, hydrographic basin of c. 1400 km^2, and annual average discharge of c. 35 m^3/s, it is one of the main rivers of central Italy. In the Acque Albule Basin, this river drains the majority of both surface and subsurface waters (Capelli et al., 1987).

Table 1
Chemical data (La Vigna et al., 2012) for the Regina Lake (see location in Fig. 2) waters. Each value is the mean of four values corresponding to four seasonal samplings during 2008.

Sampling date (year)	No. of samples	T (°C)	pH	Eh (mV)	EC (mS/cm)	Na^+ (mg/l)	K^+ (mg/l)	Ca^{2+} (mg/l)	Mg^{2+} (mg/l)	HCO^{3-} (mg/l)	SO_4^{2-} (mg/l)	Cl^- (mg/l)	As (μg/l)	PCO_2 (atm)
2008	4	22.2	6.2	−9	3.5	131	28	620	127	1616	803	154	120	0.59

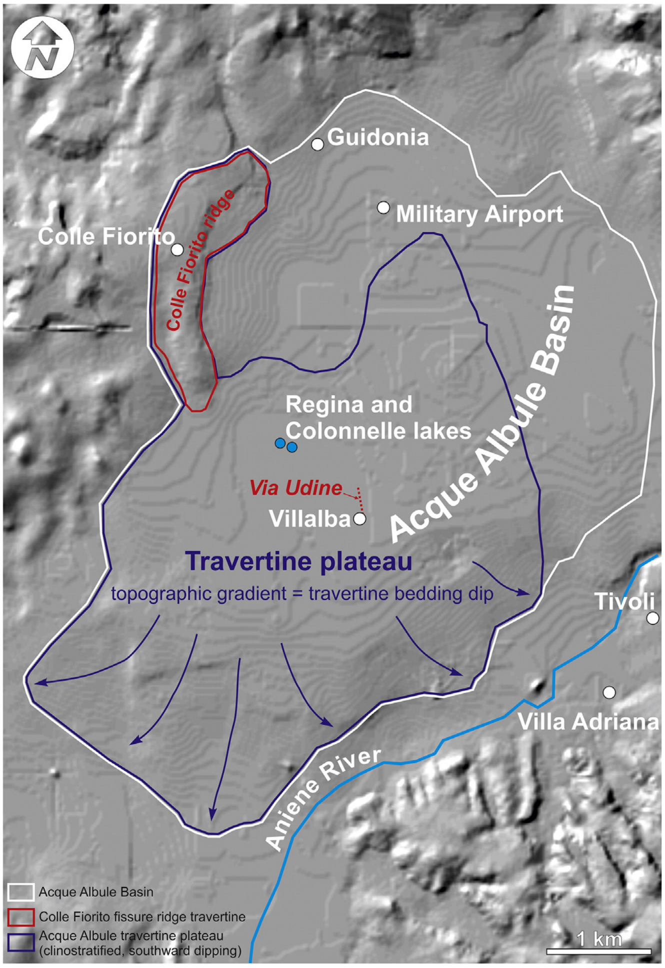

Fig. 6. Digital elevation model of the Acque Albule Basin showing the general morphology of the study area (20 m of horizontal resolution and 5 m of maximum vertical resolution). Note, in particular, the southward gentle topographic gradient of the basin corresponding to a similar gentle clinostratification dip (i.e., same direction and dip) of the travertine beds prograding toward the south. Except for the Colle Fiorito ridge (interpreted as a fissure ridge travertine in De Filippis et al., 2013a), the travertine body filling the Acque Albule Basin forms no relieved topography.

The Acque Albule Basin is affected by numerous natural depressions (sinkholes), most of which are characterized by circular or quasi-circular shapes, sharp rims in places, and diameters ranging between a few meters and almost 1 km (Fig. 7; see also Fig. 5b, d). Some of these depressions are known as present (e.g., Regina and Colonnelle lakes) or past lakes presently dried (e.g., Inferno and Tartari lakes). The depressions are particularly frequent in the areas of the Villanova, Villalba, and Castell'Arcione villages and Guidonia town, where the depressions have been mostly obliterated by the overbuilding. Other swarms of circular depressions are present in the Inferno Lake locality and in the quarry area, where these depressions have been completely obliterated by the quarrying (Fig. 7).

Further interesting geomorphic features observed in the Acque Albule Basin are small (less than about 3 m in diameter and 2 m in height) circular or quasi-circular conical or truncated-conical prominences. There are at least two main swarms of these features, which are located along the Colle Fiorito ridge and immediately to the southwest of the Guidonia airport runway (see dots in Fig. 7). As pointed out in previous work (De Filippis et al., 2013a), we interpret these features as connected with recent geothermal springs and degassing phenomena. Locality names such as “Il Bollente” (meaning “the boiling locality”) or “Acque Albule” (meaning “whitish waters”) together with other geological evidence provided by De Filippis et al. (2013a) suggest that this interpretation is correct.

Fig. 7 shows that circular depressions possibly connected with karst processes are common and widespread in the basin; however, these depressed structures are not homogeneously distributed and are apparently lacking in some areas. To understand whether in these latter areas, sinkholes and other karst structures are absent in the subsurface or otherwise are present but could not be sensed by the methods used so far by us (remote and field surveys), we choose one of these areas (i.e., the Villalba village; Fig. 7) and used subsurface geological and geophysical methods to explore the occurrence of hidden subsurface karst structures. Villalba village was chosen due to the presence of buildings, which are, in some instances, sinking and damaged, and for its high population density. The results of this second phase of investigation are described in the next section.

4. Subsurface investigation of the Villalba village

4.1. Workflow and methods

4.1.1. Workflow

For our detailed subsurface study, we chose the Via Udine locality in the Villalba village. In this locality, which is apparently lacking in (active) karst-related depressions and is richly populated and overbuilt (Figs. 5a, 7, 8a), we acquired six ERT cross-sections and completed seven penetration tests (DPSH). We calibrated the ERT cross-sections and penetration test results by running a ERT cross-section and two penetration tests in a nearby locality in the Acque Albule Basin, where the subsurface geology, which mainly consists of travertine beds affected by a large regolith-filled solution sinkhole, is exposed thanks to the presence of adjacent quarries (i.e., the quarry wall shown in Fig. 3g). Furthermore, we corroborated this calibration with results from previous ERT studies in similar settings (i.e., travertine beds affected by regolith-filled sinkholes) of the Acque Albule Basin (De Filippis et al., 2013a; Argentieri et al., 2015) and by borehole logs available for the Villalba village area, as explained below.

4.1.2. Geophysical methods

Before explaining the methods that we used in this work (see the following sections), as a reference guide, we here mention and briefly describe all the main subsurface geophysical methods so far used to investigate hidden sinkholes (for reviews and applications see Stierman, 2004; Waltham et al., 2005; García-Moreno and Mateos, 2011; Margiotta et al., 2012; Gutiérrez et al., 2014): (1) electrical resistivity (e.g., Zhou et al., 2002; Ahmed and Carpenter, 2003; Epting et al., 2009; Frumkin et al., 2011; Valois et al., 2011; Carbonel et al., 2013; Lollino et al., 2013); (2) ground penetrating radar (e.g., Batayneh et al., 2002; Tallini et al., 2006; Pueyo-Anchuela et al., 2010; Frumkin et al., 2011); (3) seismic reflection (e.g., Sargent and Goulty, 2009; Krawczyk et al., 2012); (4) seismic refraction (e.g., Higuera-Diaz et al., 2007; Frumkin et al., 2011; Valois et al., 2011; Samyn et al., 2014); (5) gravimetry (e.g., Patterson et al., 1995; Buttrick and van Schalkwyk, 1998; Matthews et al., 2000; Tuckwell et al., 2008; Kaufmann and Romanov, 2009; Argentieri et al., 2015); and (6) magnetometry (e.g., Thierry et al., 2005; Argentieri et al., 2015).

(1) In electrical resistivity surveys, which we used in this work (see the following sections), the electrical resistance of different rock masses and layers is used to detect and map subsurface geological features such as sinkholes. This method provides very clear and easy to interpret data in the case of a marked difference of electrical resistances such as the cases of sinkholes filled by air or water. In the first case, the resistivity will be very high (air) compared with that of humid surrounding rocks, whereas it will be very low in the second case (water) compared with that of the surrounding poorly-

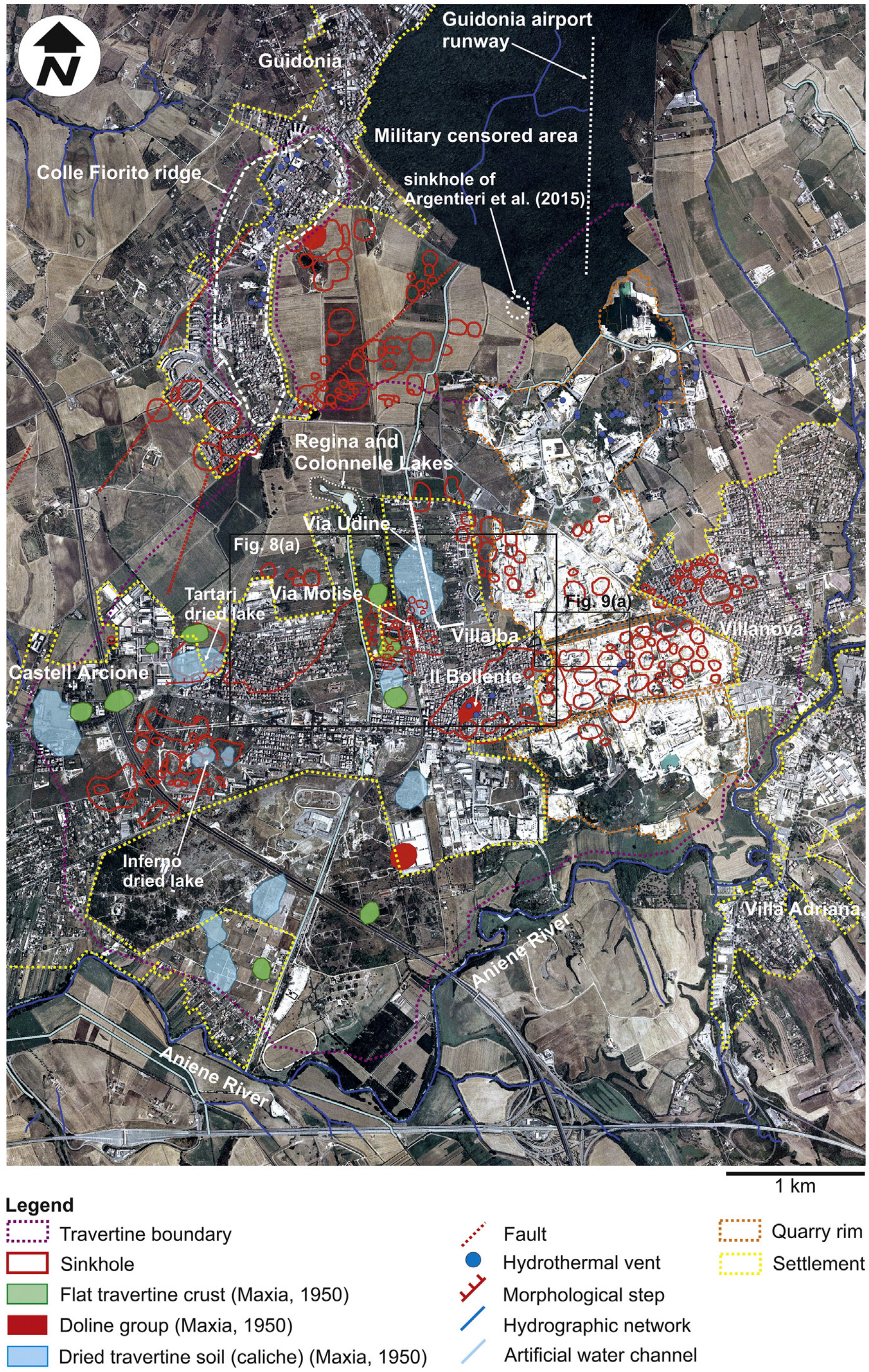

Fig. 7. Geomorphic map of the Acque Albule Basin. Morphological features are mapped over a recent aerial photograph from Google Earth. Due to the recent overbuilding and quarrying of large sectors of the Acque Albule Basin, most geomorphologic features have been detected using pre-construction and pre-quarrying material such as old aerial photographs (RAF, Royal Air Force photograph of 1943) and geomorphic maps (Maxia, 1950).

porous rock. This method has been successfully applied several times to sinkhole searches (e.g., Zhou et al., 2002).

(2) In ground penetrating radar (GPR) surveys, high-frequency (usually polarized) radio waves, normally in the 10 MHz to 1 GHz range, are transmitted into the ground. When the waves encounter a boundary between geological media having different dielectric constants, the waves are reflected, refracted, or scattered back to the surface, where a receiving antenna will record the variations in the return signal. This method can be well used in the case of geological bodies with different dielectric constants (e.g., water- or air-filled sinkholes) and has been successfully applied to sinkhole searches (e.g., Frumkin et al., 2011).

(3) Similarly to the previous method, in seismic reflection surveys, seismic waves are transmitted into the ground through a seismic source of energy such as dynamite, air gun, or seismic vibrator. The waves reflected by the boundary between geological media having different rheological properties (i.e., velocity of seismic waves) are recorded by geophones and processed to map the subsurface geological boundaries.

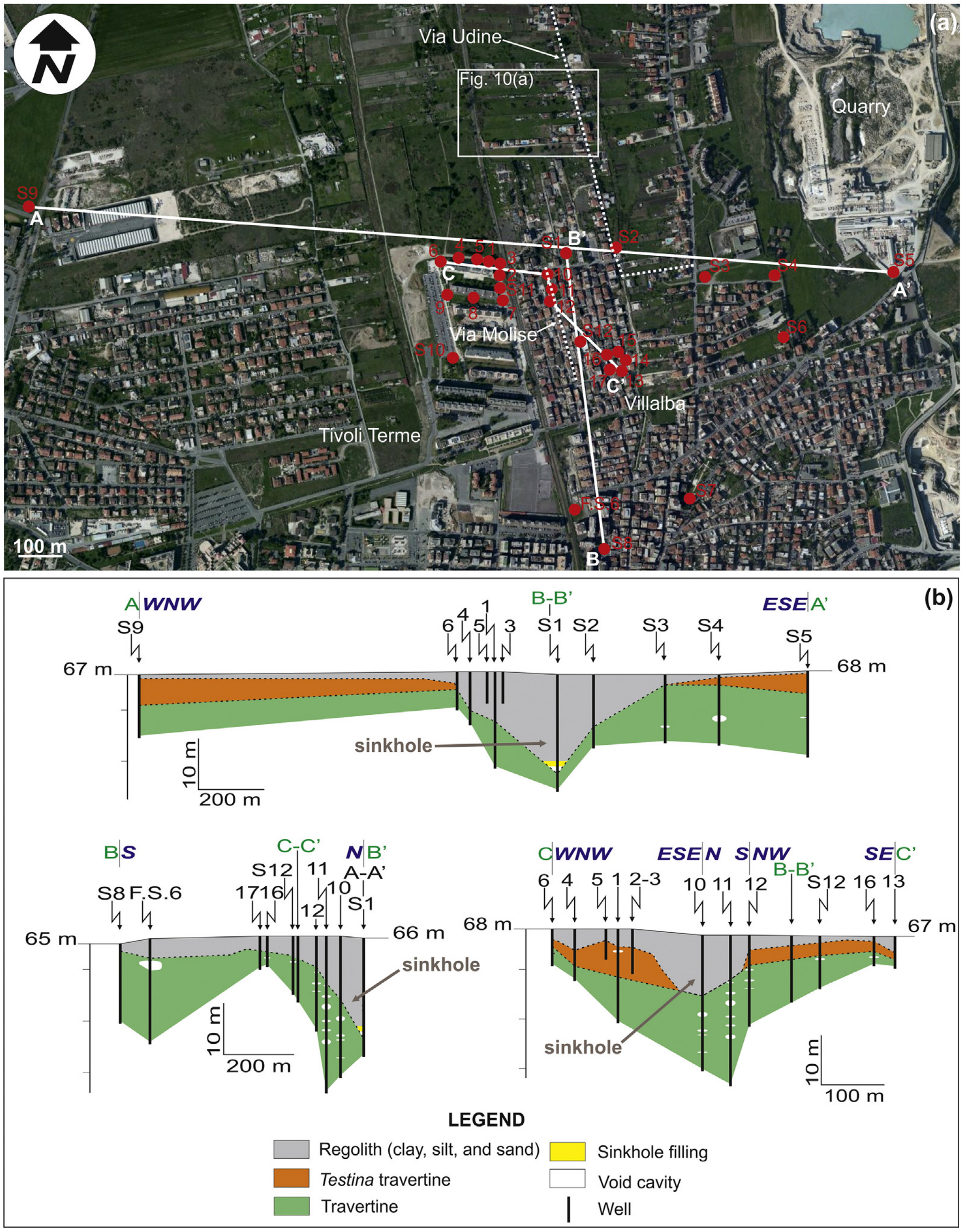

Fig. 8. (a) Location map (from Bing Maps) of boreholes in the Villalba village (Via Molise locality; see location in Fig. 5a) used to construct the borehole correlation schemes of next figure. (b) Borehole correlation schemes (see tracks in the previous figure) beneath Via Molise locality, Villalba village. Note the presence of a huge buried (hidden) solution sinkhole that is about 25 m deep.

This method is rarely used in sinkhole surveys, although some recent successful applications in this field are known (e.g., Sargent and Goulty, 2009; Krawczyk et al., 2012).

(4) Similarly to the previous method, in seismic refraction surveys, seismic waves are transmitted into the ground through a seismic source of energy. Instead of reflected waves, the seismic refraction method uses the refraction of seismic waves on geological layers to characterize the subsurface geological setting, where layers with different velocities of the seismic waves are recognized and mapped. Also this method is rarely used in sinkhole surveys, although some recent successful applications in this field are known (e.g., Higuera-Diaz et al., 2007; Frumkin et al., 2011; Valois et al., 2011; Samyn et al., 2014).

(5) In gravimetric surveys, the subsurface mass distribution is investigated and defined. Gravity surveys are based on the fact that different geological bodies can have different densities. The fundamental physical law behind this method is, in fact, that of Newton (Newton's law of universal gravitation), describing the force of attraction and therefore the acceleration between two masses within a certain distance. The gravimetric method has been successfully applied in the case of sinkholes empty (filled by air) or filled by water or by loose material (regolith) with density markedly lower than the density of the host rock (e.g., Argentieri et al., 2015).

(6) In magnetic surveys, the spatial variation of the Earth's magnetic field is recorded to detect and map geological features characterized by a differential in the magnetic properties. Magnetic

surveys may use a single sensor to determine the total magnetic field strength or may use two or more separated sensors to determine the gradient of the magnetic field. The magnetic method is rarely used in sinkhole surveys for the slight differences in the magnetic properties of sinkhole filling and host rock; however, some recent successful applications to this field are known (e.g., Thierry et al., 2005; Argentieri et al., 2015).

4.1.3. Borehole stratigraphic logs

Unfortunately, in the Via Udine locality, there are no borehole logs available to draw a general setting of the subsurface geology; however, we were able to find a good set of borehole logs for a locality about 400 m to the south of Via Udine, namely in the Via Molise locality of the Villalba village (Fig. 8a). The logs come from the technical office building of the local municipality and we show them in three cross-

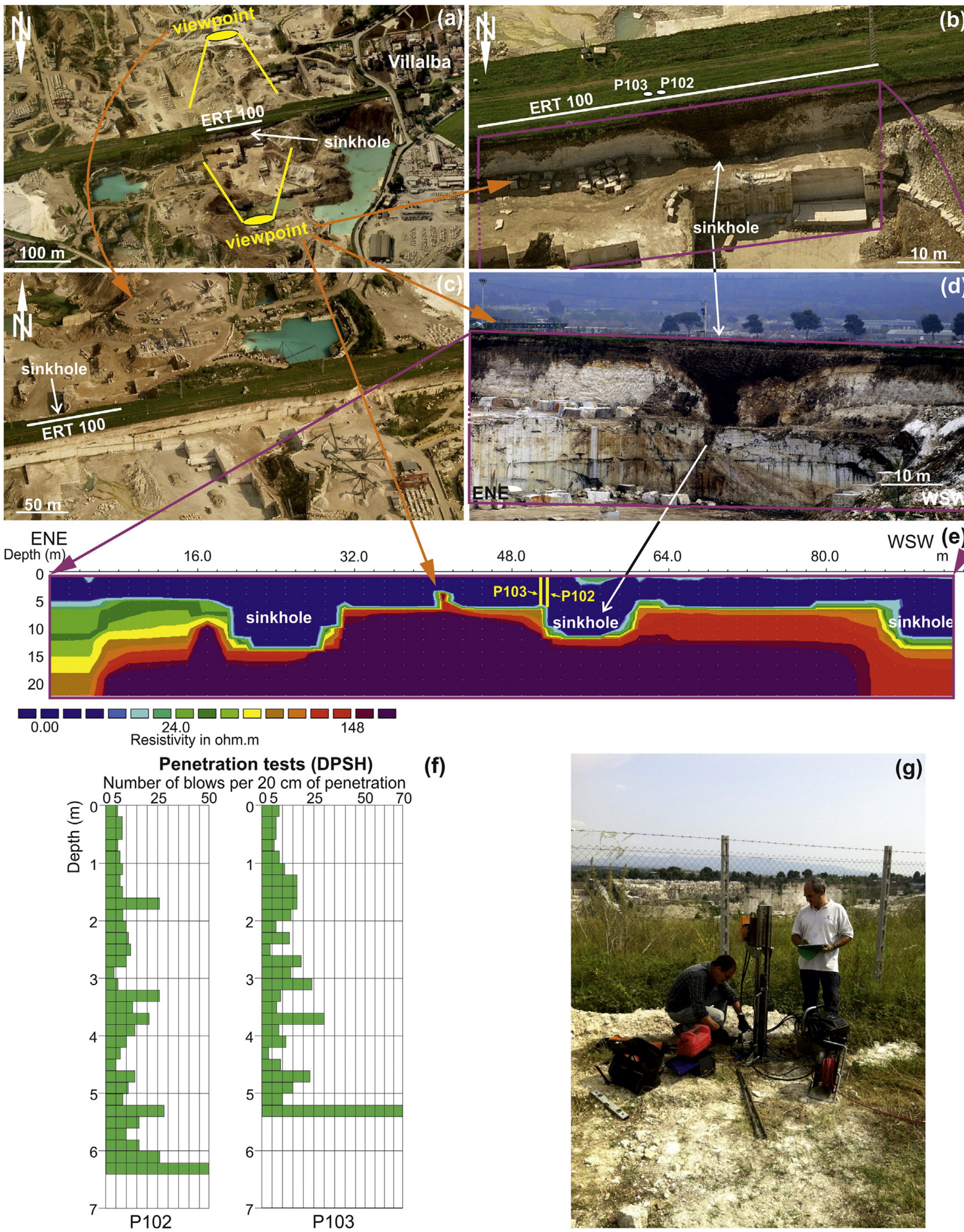

Fig. 9. Calibration of electrical resistivity tomography (ERT) cross-sections and penetration measurements (DPSH). (a), (b), (c), and (d): location map of ERT 100 (Table 2) and penetration tests P102 and P103 (Table 3) in the quarry area of the Acque Albule Basin (see Fig. 7 for location). Note in (c) and (d) the presence of at least one huge solution sinkhole filled by allogenic brown sediments. (e) ERT 100 cross-section acquired on top of the huge filled sinkhole (see ERT 100 track in previous figures). (f) Results from P102 and P103 penetration tests (dynamic probing super heavy, DPSH). The diagrams show number of blows per 20 cm of vertical penetration (horizontal) vs. depth (vertical). See test location in (a). Comparing the photographs with the penetration and ERT results, it is inferred that the travertine top occurs where the number of blows per 20 cm of vertical penetration is greater than 50–70 and where the electrical resistivity is larger than 20 Ω m. (g) P. Sella (left) and A. Billi (right) while calibrating and probing this calibration site.

sectional correlation schemes that mimic subsurface geological cross-sections (Fig. 8b). These logs are useful to know the shallow subsurface setting of the Villalba village and to correctly interpret the ERT cross-sections (Figs. 9, 10, 11), which we acquired in a presumably similar setting. We acknowledge that, for these borehole logs, only the stratigraphic data and descriptions (depth and lithology) are available. No further instrumental borehole data are available.

4.1.4. Electrical resistivity method (ERT)

We used the ERT method to obtain information about the lateral and vertical distribution of shallow rock resistivity in the Via Udine locality. We determined the subsurface resistivity distribution by making measurements on the ground surface with an electrical device. We then estimated the true resistivity distribution of the subsurface rocks from these measurements (Barker, 1992). The geoelectric method can

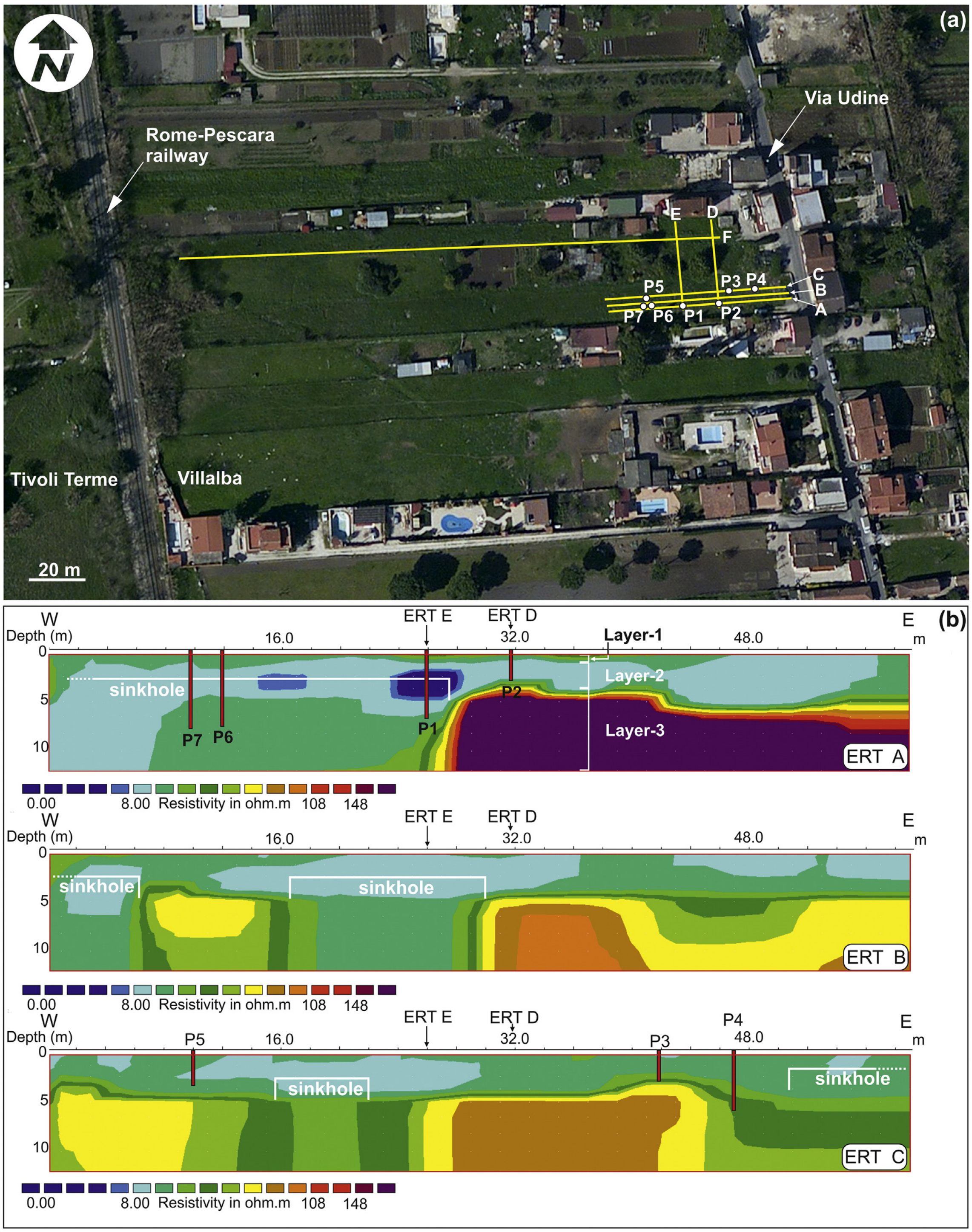

Fig. 10. (a) Location map (see area location in Fig. 8a) for six ERT (electrical resistivity tomography) cross-sections (Table 2) and seven DPSH penetration tests (Table 3) shown in this figure and in Fig. 11 (Via Udine locality, Villalba village). (b) ERT cross-sections. The travertine basement (undifferentiated testina plus compact travertine) is represented by a resistivity greater than circa 20 Ω m as also demonstrated by the penetration tests (Fig. 11b). Depressions of the resistivity isolines are indicated as possible clay-filled sinkholes. Some of these structures could be better defined as clay-filled caves or cavities that may become future sinkholes. Layer-1 is made of anthropic backfill and/or travertine surface crusts (caliche). Layer-2 is a low-resistivity layer probably made of clay-rich regolith and soil. Layer-3 is a high resistivity layer starting at about 5 m depth and it is made by the main travertine body (testina and compact travertines).

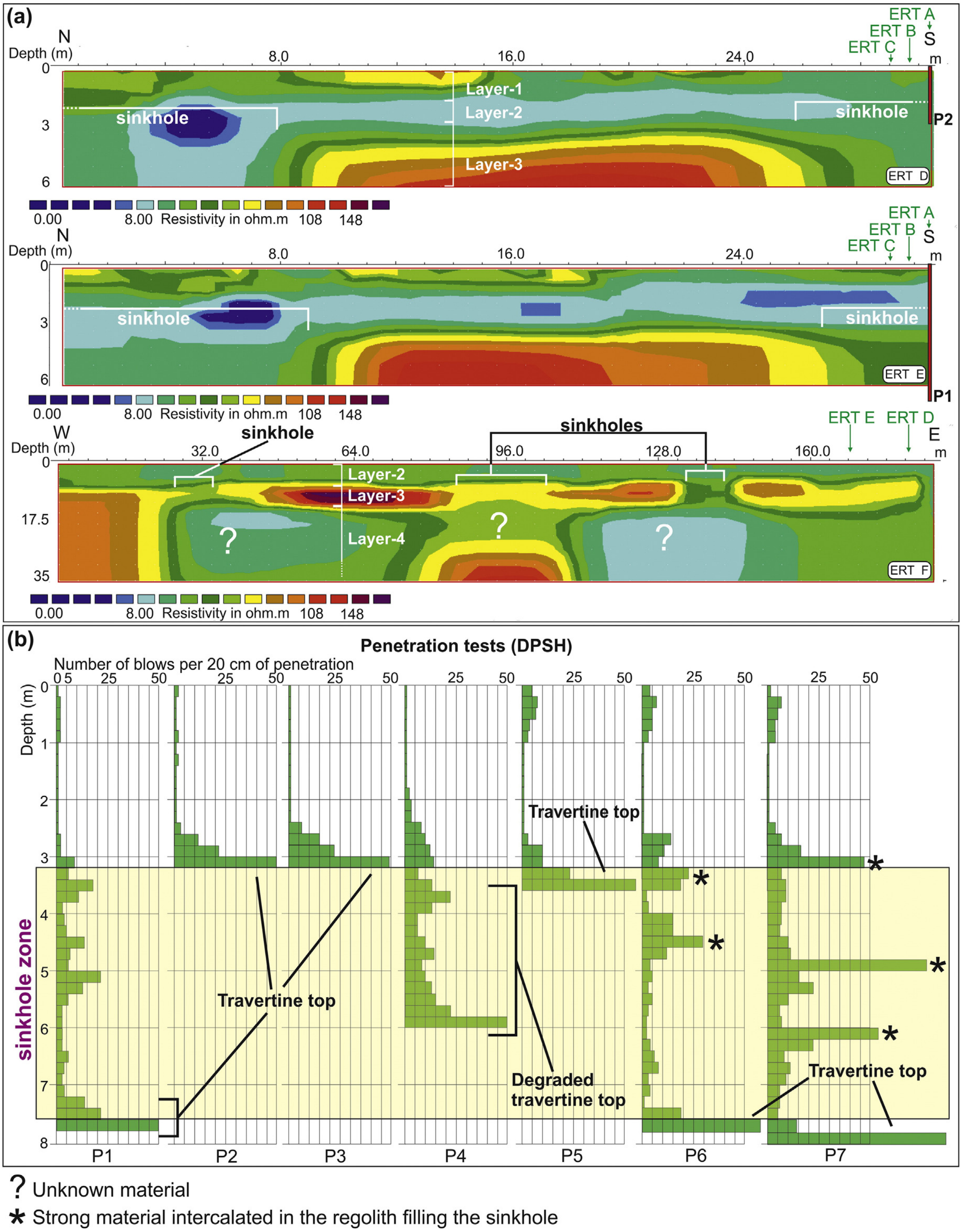

Fig. 11. (a) ERT cross-sections (see location in Fig. 10a and Table 2). The travertine basement (undifferentiated testina plus compact travertine) is represented by a resistivity greater than circa 20 Ω m as also demonstrated by the penetration tests (Fig. 11b). Depressions of the resistivity isolines are indicated as possible sinkholes. Some of these structures could be better defined as clay-filled caves or cavities that may become future sinkholes. Note the different lengths and depths of the cross-sections (Table 2). Layer-1 is made of anthropic backfill and/or travertine surface crusts (caliche). Layer-2 is a low-resistivity layer probably made of clay-rich regolith and soil. Layer-3 is a high resistivity layer starting at about 5 m depth and it is made by the main travertine body (testina and compact travertines). Layer-4 occurs at depths deeper than c. 17.5 m and could be ascribed to the presence of low resistivity rocks such as clays (filling caves?) or to the presence of the unconfined aquifer in the travertine (La Vigna et al., 2013b) or both. Groundwater in the Acque Albule Basin is, in effect, characterized by high mineralization (circa 3.5 g/l; La Vigna et al., 2012), which can strongly influence (reduce) rock electric resistivity. (b) Results from dynamic probing super heavy (DPSH) tests (i.e., number of blows per 20 cm of vertical penetration vs. depth). See test location in Fig. 10(a) and Table 3. The top of the travertine layer (Layer-3) is usually at c. 3 m depth except where sinkholes occur increasing the depth at which the travertine top occurs (i.e., see the shading indicating the sinkhole zone).

identify rock layers and masses of significantly different resistivities such as clays, marls, sands, sandstones, limestones, and water-saturated soils and rocks. For this reason, this method is one of the most frequently used for site investigation in karst areas (e.g., Zhou et al., 2000; Schwartz and Schreiber, 2009; Youssef et al., 2012; Martínez-Moreno et al., 2013; Carbonel et al., 2014a,b), particularly where the regolith overlying the carbonate is clay-dominated (Cook and Van Nostrand, 1954), as it occurs in the Via Udine locality. The electrical resistivity of carbonate rocks is, in general, significantly higher than the one of clayey soil and regolith because carbonates have much smaller primary porosity and fewer interconnected pore spaces. The resistivity is slightly reduced in travertines with respect to marine carbonates. Travertines are, in effect, carbonate rocks that can be significantly more porous than marine compact limestone (Ronchi and Cruciani, 2015). The resistivity contrast between travertine and clayey sediments is, however, marked, with travertine being characterized by a resistivity over about 20–25 Ω m and clayey regolith by a resistivity in the 0–15 Ω m range (De Filippis et al., 2013a). As a comparison term, we acknowledge that, in a similar setting within the Acque Albule Basin, Argentieri et al. (2015) have recently found that the resistivity of a sinkhole-filling regolith (calibrated through in situ direct investigations in holes digging down into the filled sinkhole) is in the 0–20 Ω m range, whereas the resistivity of the host travertine is over 20–25 Ω m. Such a contrast in resistivity values favored the use of the resistivity method to delineate the boundary between the travertine bedrock and clayey overburden (regolith) below Via Udine (Figs. 10, 11).

We acquired the ERT cross-sections using a PASI (16S24N model) electrical device enabling the use of up to 48 electrodes. We used the 32- and 48-electrodes settings depending on the site conditions. We varied the separation between electrodes between 1 and 4 m so to realize resistivity sections of different lengths (32 to 188 m) and depths (6 to 35 m) (Table 2). In each cross-section, we applied both the Wenner and the Schlumberger electrode configuration (Loke and Barker, 1996; Loke, 1996), carrying out the measurements at a constant potential (voltage) up to a maximum of 300 V.

We inverted the acquired data using RES2DINV (Loke, 1999), an inversion routine based on the smoothness-constrained least squares method (DeGroot-Hedlin and Constable, 1990). This method attempts to minimize the square of the changes in the model resistivity values and to smooth the boundaries. As a result, a model with a smooth variation in the resistivity values is obtained. The principle of the inversion procedure is as follows (Zohdy, 1989; Loke, 1999): in-situ measured apparent resistivities are introduced into the software as input data. The program generates initial 2D true resistivity model and calculates an apparent resistivity pseudo-section using forward modeling software. Measured and calculated pseudo-sections are compared while the program corrects the true resistivity section. A new pseudo-section is then calculated and compared again with the measured one. By varying the inverse resistivity section through multiple iterations, the program fits the calculated apparent resistivity pseudo-section into the measured one. In this manner, the program minimizes the Root Mean Square (RMS) error. The final outputs of the inversion process are: (1) a measured apparent resistivity pseudo-section, (2) a calculated apparent resistivity pseudo-section, and (3) a corresponding true resistivity model. In this work, we show only the models (Figs. 9, 10, 11) and acknowledge that the final RMS error, which is the difference between the successive two-dimensional model inversions and the measured data, is less than 6% for all ERT cross-sections. The acquisition parameters of all ERT cross-sections are reported in Table 2.

4.1.5. Penetration method (DPSH)

We performed a set of dynamic penetration tests using a percussion penetrometer (e.g., Terzaghi et al., 1996; Lunne et al., 1997; Salgado and Yoon, 2003; Sudha et al., 2009; Jung et al., 2011; Wiegand et al., 2013). This type of test allows operators to evaluate, in a fast and cheap manner, the mechanical properties (in-situ resistance to penetration) of surface and subsurface soils and soft rocks. More specifically, in this work, we used a penetration method named DPSH (dynamic probing super heavy), where a load (hammer) of 63.5 kg dropping from 75 cm is used (e.g., MacRobert et al., 2010, 2011). The percussion penetrometer consists of upper and lower shafts. The upper shaft has a drop load (hammer) that strikes on the lower shaft through an anvil situated at the upper end of the lower shaft. The lower penetrating end of the lower shaft consists of a replaceable cone to lose with a 60° cone angle and a 50.46 mm cone diameter. Each shaft is 1 m long and weighs 6.3 kg. A bar with marks at known distances is used as reading device along the lower shaft (i.e., number of blows for 20 cm of vertical penetration). Hammer blows are repeated to cause the penetration of the lower shaft while the penetration depth is measured for each hammer drop. This process is continued until a desired penetration depth is reached or an impenetrable rock is hit (e.g., the travertine substratum). DPSH results consist of number of blow counts versus penetration depths (i.e., number of blow counts for each 20 cm of penetration in this work; Figs. 9f, 11b). The number of blow counts provides an indirect measurement of the soil or rock stiffness. DPSH is an optimal, fast, and cheap method to distinguish underground soils or rocks with highly contrasting stiffness as is the case of this work, where the travertine substratum and the overlying regolith (loose clay and sand) are remarkably different in stiffness (e.g., see Mendonca et al., 1993, for penetration tests run in a regolith-filled sinkhole-rich area). We used the DPSH results to test results from the ERT cross-sections (Figs. 9, 10, 11). As is explained below, we calibrated the DPSH results by running two tests in a site where the subsurface geology is partly exposed (the quarry wall

Table 2
Acquisition parameters for the ERT cross-sections shown in Figs. 9, 10, and 11.

ERT cross-section	Fig.	End 1: latitude, longitude	End 2: latitude, longitude	No. of electrodes	Electrode separation (m)	Total length (m)	Penetration depth (m)	Maximum recorded resistivity (Ω m)
100 (calibration)	9	41° 57.542′ N 12° 44.515′ E	41° 57.555′ N 12° 44.580′ E	48	2	94	21	Circa 55
A	10(b)	41° 57.771′ N 12° 43.636′ E	41° 57.773′ N 12° 43.681′ E	32	2	62	12	Circa 300
B	10(b)	41° 57.773′ N 12° 43.636′ E	41° 57.775′ N 12° 43.681′ E	32	2	62	12	Circa 100
C	10(b)	41° 57.774′ N 12° 43.635′ E	41° 57.776′ N 12° 43.680′ E	32	2	62	12	Circa 100
D	11(a)	41° 57.789′ N 12° 43.663′ E	41° 57.772′ N 12° 43.665′ E	32	1	31	6	Circa 175
E	11(a)	41° 57.789′ N 12° 43.654′ E	41° 57.772′ N 12° 43.656′ E	32	1	31	6	Circa 500
F	11(a)	41° 57.783′ N 12° 43.532′ E	41° 57.787′ N 12° 43.668′ E	48	4	188	35	Circa 2500

shown in Fig. 3g). The acquisition parameters of all penetration tests are reported in Table 3.

4.1.6. ERT and DPSH calibration

We acquired ERT and DPSH data in a calibration locality (Fig. 9, Tables 2, 3) so to better understand and interpret the ERT and DPSH results from the Via Udine locality (Figs. 10, 11). The calibration locality is right on top of a huge quarry wall, where the travertine beds and at least one large regolith-filled sinkhole are magnificently exposed (Fig. 9a–d). With this calibration procedure, we intended to minimize the possibility of misinterpreting the ERT and DPSH penetration data from the Via Udine locality (Figs. 10, 11). The calibration is also corroborated by previous ERT data acquired in the Acque Albule Basin in similar settings (i.e., travertine hosting sinkholes filled by clayey regolith; De Filippis et al., 2013a; Argentieri et al., 2015).

The electrical resistivity pattern of the ERT cross-section (Fig. 9e) shows the presence of two main (rock) domains: a shallow one characterized by an electrical resistivity lower than circa 10 Ω m and a deep one characterized by an electrical resistivity larger than circa 50 Ω m. A rather narrow transitional area, characterized by an electrical resistivity between about 10 and 50 Ω m, separates the two main resistivity domains. By comparing the ERT cross-section with the corresponding rock exposure (Fig. 9e vs. b, d), we infer that the low resistivity domain (0–10 Ω m) corresponds to shallow regolith mainly made of clayey and sandy allogenic deposits whereas the high resistivity domain (≥50 Ω m) corresponds to the underlying travertine. The transitional zone (10–50 Ω m) is more complicated to be interpreted. The penetration results (Fig. 9e, f) show that the impenetrable travertine (more than 50–70 blows per 20 cm penetration) corresponds exactly to an electrical resistivity of 20 Ω m and greater, but the number of blows significantly increases (over 20–25 blows per 20 cm penetration) already for an electrical resistivity larger than about 10 Ω m. We conclude that the top of the impenetrable travertine occurs at an electrical resistivity of about 20 Ω m; however, the occurrence, on top of the impenetrable travertine, of a more porous or degraded travertine (e.g., Figs. 3b, 4d) as well as the presence of travertine breccias (e.g., Fig. 4b, e) may slightly change the above defined threshold (20 Ω m). It is also known that the same rock can sensibly change its electrical resistivity depending upon numerous factors including fluid saturation. We therefore assess and expect that the top of the impenetrable travertine should probably occur at electrical resistivities larger than about 10–20 Ω m and surely at electrical resistivities larger than about 50 Ω m. These conclusions are consistent with results from De Filippis et al. (2013a) and Argentieri et al. (2015), for whom the top of the travertine bedrock in the Acque Albule Basin occurs at circa 20–25 Ω m and greater.

Table 3
Acquisition parameters for the DPSH penetration tests shown in Figs. 9 and 11.

Penetration test	Fig.	Latitude, longitude	Depth (m)
P102 (calibration)	9(f)	41° 57.554′ N 12° 44.561′ E	6.4
P103 (calibration)	9(f)	41° 57.554′ N 12° 44.562′ E	5.4
P1	11(b)	41° 57.772′ N 12° 43.656′ E	7.8
P2	11(b)	41° 57.773′ N 12° 43.665′ E	3.2
P3	11(b)	41° 57.776′ N 12° 43.669′ E	3.2
P4	11(b)	41° 57.776′ N 12° 43.675′ E	6.0
P5	11(b)	41° 57.774′ N 12° 43.649′ E	3.6
P6	11(b)	41° 57.772′ N 12° 43.651′ E	7.8
P7	11(b)	41° 57.772′ N 12° 43.648′ E	8.0

It is also important to note that the shallow domain (soft regolith) in Fig. 9 is characterized by heterogeneous penetration profiles with a number of blows per 20 cm penetration up to circa 30 (Fig. 9f). We interpret this result with the presence of pockets or blocks of strong material such as breccias or travertine cement and crusts in the regolith domain. This interpretation is based on direct observations of other filled karst cavities in the Acque Albule Basin (e.g., Figs. 3, 4).

Eventually, from the presented calibration scheme, it is rather obvious that the ERT method (together with DPSH results) is suitable and reliable in sinkhole investigations. The main central sinkhole and at least other two smaller ones visible in Fig. 9(b) and (d) are, in effect, well represented by the electrical resistivity pattern of Fig. 9(e).

4.2. Results

The studied boreholes are between a few meters and c. 30 m deep (Fig. 8b). From bottom to top, the stratigraphy of the area is characterized by: (1) the local compact lithoidal travertine (late Pleistocene), which is overlain by (2) the porous and poorly lithoidal testina travertine (late Pleistocene) or directly by (3) regolith, present soil, and anthropic backfill (Holocene), which, in turn, can also cover the testina travertine. The base of the compact travertine is unknown although it should not exceed a few tens of meters below the surface (Faccenna et al., 2008). The thickness of the testina is variable between a few decimeters and a maximum of 13 m (Fig. 3b), whereas the overlying regolith is between a few decimeters and a few tens of meters depending on the karstic shaping of the underlying travertines. Empty or clay-filled cavities are frequent in the travertine deposits (Figs. 3, 4). Fig. 8(b) shows a distinct and obvious incision of these travertine deposits. The incision, which is more than 500 m wide and about 25 m deep, is filled by regolith. It is interesting to note that this incision, which we interpret as a buried solution sinkhole (cf. Fig. 1a), lies exactly beneath the densely populated Villalba village, particularly beneath the Via Molise locality, where most building damages and road depressions have been observed (Brunetti et al., 2013; De Filippis et al., 2013c).

The ERT cross-sections acquired in the Via Udine locality (Figs. 10b, 11a) show a resistivity pattern including, from top to bottom: (1) Layer-1: it is a high resistivity layer (10–200 Ω m) that occupies the shallowest portion of the cross-sections for less than about 1 m thickness (e.g., ERT A and D in Figs. 9b and 10a, respectively); (2) Layer-2: it is a low resistivity layer (0–10 Ω m) that lies at about 2.5–3.0 m depth (e.g., ERT A in Fig. 9b); (3) Layer-3: it is a high and thick resistivity layer (10–2500 Ω m) starting at about 5 m depth and downward extending for a few meters (e.g., ERT A in Fig. 9b); (4) Layer-4: it is a low resistivity layer (0–20 Ω m) that occupies the deepest portion (deeper than 17.5 m) of ERT F in Fig. 10a.

From top to bottom, with the aid of the calibration tests (Fig. 9), seven DPSH penetration test results (Fig. 11b), borehole logs (Fig. 8), and borehole-calibrated ERT cross-sections previously acquired in similar settings of the Acque Albule Basin (De Filippis et al., 2013a; Argentieri et al., 2015), we interpret these layers as follows.

(1) Layer-1 is probably made of anthropic backfill and/or travertine surface crusts (caliche).
(2) Layer-2 is a low-resistivity layer probably made of clay-rich regolith and soil. The penetration tests (Table 3) show that this electrical low resistivity material is also low in resistivity to penetration; however, blocks of material resistant to penetration occur in this layer in correspondence of the penetration tests P6 and P7 (Figs. 10b, 11b). We do not know the lithological nature of these blocks and hypothesize that they could be travertine blocks, breccias, and/or cement filling sinkholes as observed in the quarry exposures (Figs. 3, 4).
(3) Layer-3 is a high resistivity layer starting at about 5 m depth and it is made by the main travertine body (testina and compact travertines).

(4) We cannot interpret the low resistivity Layer-4 occurring at depths deeper than circa 17.5 m in the ERT F (Fig. 11a). This low resistivity could be, in effect, ascribed to the presence of low resistivity rocks such as clays or to the presence of large cavities filled by clayey deposits. The presence of the unconfined aquifer in the travertine (La Vigna et al., 2013b) may also partially reduce the resistivity of this layer. Groundwater in the Acque Albule Basin is, in effect, characterized by high mineralization (circa 3.5 g/l; La Vigna et al., 2012), which can strongly influence (reduce) rock electrical resistivity.

5. Discussion and conclusions

Our research on and brief discussion of hidden sinkholes in the Acque Albule Basin focus on human-environment interaction and eventually aim at evaluating the general significance of results including practical and policy applications without expanding, if not superficially, on the topic of the sinkhole driving processes. To do so, in this section, first we interpret our data from the Via Udine locality and then discuss these results framing them within the Acque Albule Basin surface processes. We conclude with some insights into the management of such a densely-populated land of sinkholes and active geological processes and human works.

Based on the calibration tests (Fig. 9), borehole logs (Fig. 8), available exposures (Figs. 3, 4), and previous subsurface studies in the Acque Albule Basin (De Filippis et al., 2013a; Argentieri et al., 2015), we interpret our ERT and DPSH penetration data (Figs. 10, 11) from the Via Udine locality as consisting of a travertine substratum (Layer-3 in Figs. 10, 11) lying at depths equal or larger than about 3 m below two covering layers consisting of anthropic backfill, travertine surface crusts (caliche), and, in general, soft regolith (i.e., Layer-1 and Layer-2 in Figs. 10, 11). The travertine substratum has a good lateral continuity (electrical resistivity greater than about 20 Ω m in Figs. 10b, 11a) that is, however, interrupted in places. As demonstrated by both ERT and penetration data, these interruptions are characterized by a downward thickening of the regolith and consistent deepening of the travertine top surface down to circa 8 m (P1 in Fig. 11b) or even deeper (ERT F in Fig. 11a). The lateral correlation of penetration results (i.e., number of blows per 20 cm vs. depth), in particular, shows that the travertine top surface is, in places, depressed down to about 6–8 m depth from its minimum depth of about 3 m (Fig. 11b).

Comparing our ERT and penetration data from the Via Udine locality with exposures from the near travertine quarry walls (Figs. 3, 4, 9) and with borehole logs from the near Via Molise locality (Fig. 8), we interpret the lateral interruptions of Layer-3 in the ERT cross-sections as a series of shallow clay-filled sinkholes affecting the travertine substratum in Via Udine as happens in the case of the exposed travertine-hosted sinkhole of Fig. 9. Some of these structures could be better defined as clay-filled caves or cavities that may become future sinkholes. We do not know exactly the origin of these sinkholes as they could be either cave-collapse or solution sinkholes (Figs. 1, 12) of the type observed on the quarry exposures (Figs. 3, 4). In Fig. 11(b), we collectively name the travertine depressed sectors between 3 and 8 m as the 'sinkhole zone'. The presence, in this zone, of blocks highly resistant to the penetrometer conical head (see P6 and P7 in Fig. 11b) makes the interpretation of this zone complex, indicating the probable occurrence of resistant blocks, fragments, breccias, or cemented layers within the filling matrix (regolith) of the sinkhole zone, as it is often observed in many exposed sinkholes (e.g., Fig. 4; Song et al., 2012).

We emphasize the fact that the sinkholes shown in Fig. 7 are at present mostly masked by quarrying and human settlements, whereas those ones discovered in the subsurface of the Via Udine locality (Figs. 10, 11) were previously unknown and totally hidden to the resolution of other used methods such as aerial photographs, DEMs, and field surveys. Our new data (Figs. 7–11), in particular, together with other previous evidence (e.g., Figs. 3, 4, 5), show that the Acque Albule Basin is a karst land where sinkholes, focused subsidence as well as seismic and hydrothermal processes are active or recently-active (e.g., Maxia, 1950; Gasparini et al., 2002; Caramanna et al., 2008; Faccenna et al., 2008; Amanti and Nisio, 2013; Brunetti et al., 2013; De Filippis et al., 2013a; Floris et al., 2014; Argentieri et al., 2015; Bozzano et al., 2015). Sinkholes and related subsidence, in particular, are active over large sectors of the Acque Albule Basin as observed on photographic and geomorphologic materials recorded before the substantial overbuilding and quarrying of the study area (Figs. 5, 7). Hydrothermal springs are active in the Colonnelle and Regina lakes and many other localities of the basin (Capelli et al., 1987), but must have been recently active also elsewhere in the basin, as evidenced by dried travertine lakes or degassing conical structures such as those observed in the 1943 aerial photographs on the Colle Fiorito fissure ridge by De Filippis et al. (2013a) (see also Maxia, 1950).

In a recent study, Argentieri et al. (2015) showed the development of a rapidly evolving (subsiding) elliptical sinkhole (c. 220 by 110 m in horizontal size) located in the Acque Albule Basin only about 1.5 km from Via Udine (see location in Fig. 7). The sinkhole was totally hidden and apparently inactive until at least all the 19th Century and probably more recently. The sinkhole began to be expressed at the surface roughly in the 2000s and continued slowly to evolve until spring 2013 when its development (subsidence) accelerated dramatically. This important case history (Argentieri et al., 2015) corroborates our suggestion that the Acque Albule Basin is a land of sinkholes and other active geological processes. Many sinkholes are manifest and visible with standard methods of Earth's surface observations; some other sinkholes, however, are hidden and apparently inactive, but can unexpectedly reactivate at any time.

The main conclusive message arising from the geomorphologic study of the Acque Albule Basin is that sinkhole activity in anthropically exploited and inhabited areas can be masked by constructions, villages, quarries and other human works that are obviously exposed at great risk for this shallow subsurface erosional activity. Even where the sinkholes are filled and apparently inactive or hidden, rejuvenation processes may reactivate these sinkholes making them an almost inexhaustible source of hazard for humans and human works. We here consider regolith suffosion and compaction among other possible sinkhole-rejuvenating-processes (Fig. 12). The anthropic masking of potentially rejuvenating sinkholes has to be carefully considered by both geoscientists and officials in charge of the environment management. In this paper, we have demonstrated that the sinkhole anthropic masking can be efficiently "unmasked" using two main strategies:

(1) where available, which is often the case in densely-populated areas, past and historical documents have to be searched, found, and carefully studied. Moreover, also collecting memories of elderly inhabitants may provide fundamental information. In the case of the Acque Albule Basin, past and historical documents (pre-edification and pre-quarrying) such as aerial photographs flown by the RAF and old geomorphologic studies (Maxia, 1950) together with memories from the elderly population allowed us to compile a geomorphologic map (Fig. 7) rich in sinkholes and geothermal springs-degassing structures, which are now completely obliterated but potentially active or re-activable;
(2) where previous studies, such as those mentioned in the latter point, evidenced the presence of potentially active sinkholes, then detailed subsurface studies such as those performed in this study in the Via Udine and Via Molise localities (using, for instance, boreholes, geophysical prospecting, and penetration tests) should be accomplished. This second strategy of sinkhole investigation is luckily becoming a standard in many sinkhole-prone areas as also demonstrated by numerous previous scientific papers (Zhou

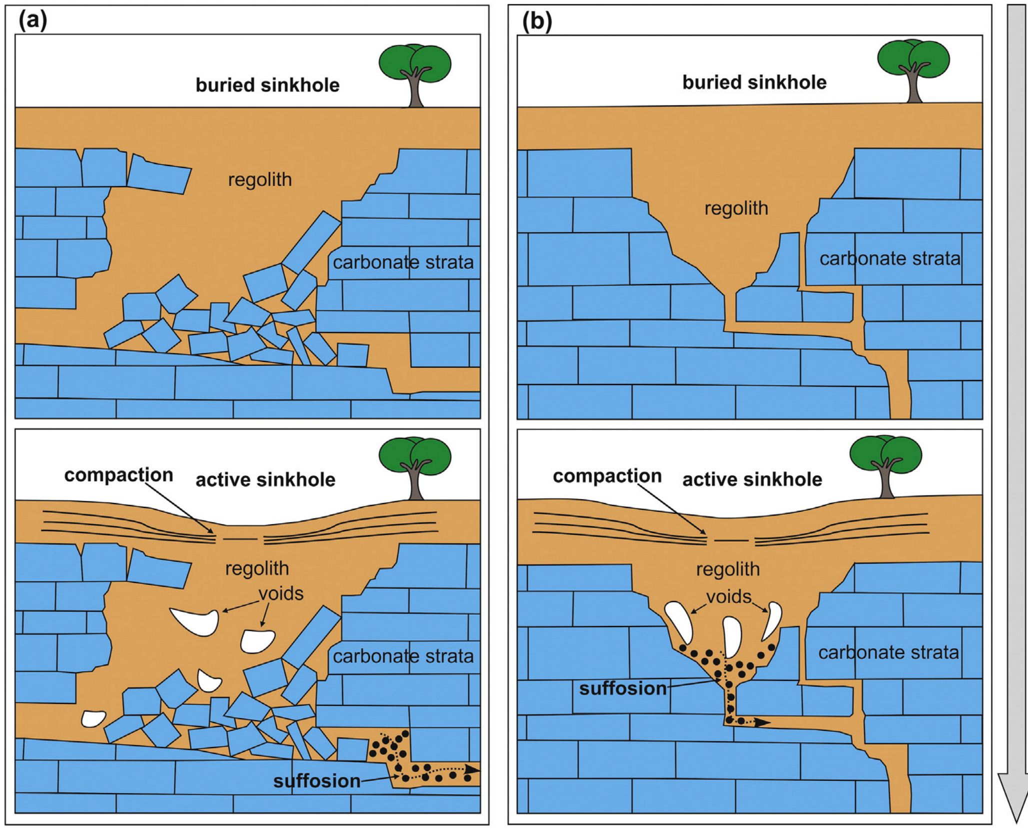

Fig. 12. (a) and (b) (top) Two types of buried (hidden) sinkholes shown in Fig. 1. (bottom) In both cases, sediment compaction, suffosion, and other processes may lead to the sinkhole rejuvenation with formation of a new surface depression (cover-subsidence sinkholes). Hydrothermal fluid circulation and pressurization or seismic shaking may enhance sinkhole rejuvenation in hydrothermal-seismic areas as is the case of the Acque Albule Basin.

et al., 2000; Ezersky, 2008; Martínez-Moreno et al., 2013; Carbonel et al., 2014a; Argentieri et al., 2015).

In synthesis, the mitigation of sinkhole hazard in highly populated areas such as the Acque Albule Basin has to pass through a thorough search of (hidden) sinkholes that can be masked by the anthropic molding and blanketing of the territory. For these purposes, instruments such as historical pre-setting documents as well as, where possible, geophysical subsurface investigations are fundamental.

Acknowledgments

This research was partly funded (general geomorphology of the Acque Albule Basin) by CVTR, Centro per la Valorizzazione del Travertino Romano (Tivoli, Rome, Italy; contract no. 2006_17: "Indagini geologiche, strutturali, stratigrafiche e idrogeologiche nell'area di Tivoli Terme (RM) e Villalba di Guidonia (RM)") and logistically–instrumentally (geophysical facilities and subsurface investigations at Villalba) supported by Geomagellan (Montecompatri, Rome, Italy). AB thanks C. Doglioni and S. Nisio for fruitful discussions on sinkholes, particularly clepsydra-like sinkholes as CD calls them. We warmly thank A. Plater and three anonymous reviewers for constructive comments and editorial handling.

Appendix A. Supplementary data

Supplementary data associated with this article can be found in the online version, at doi:http://dx.doi.org/10.1016/j.geomorph.2015.12.011. These data include Google map of the most important areas described in this article.

References

Acocella, V., Funiciello, R., 2006. Transverse systems along the extensional Tyrrhenian margin of central Italy and their influence on volcanism. Tectonics 25, TC2003. http://dx.doi.org/10.1029/2005TC001845.

Ahmed, S., Carpenter, P.J., 2003. Geophysical response of filled sinkholes, soil pipes and associated bedrock fractures in thinly mantled karst, east-central Illinois. Environ. Geol. 44, 705–716.

Amanti, M., Nisio, S. (Eds.), 2013. The Sinkholes: Methodologies of Investigation, Historical Research, Monitoring and Technique of Intervention. Towns and Natural Processes of Instability: Evaluation, Monitoring and Mitigation. Memorie Descrittive della Carta Geologica d'Italia 93 (440 pp.).

Argentieri, A., Carluccio, R., Cecchini, F., Chiappini, M., Ciotoli, G., De Ritis, R., Di Filippo, M., Nezza, D., Marchetti, M., Margottini, S., Materni, V., Meloni, F., Nardi, A., Rotella, G., Sapia, V., Venuti, A., 2015. Early stage sinkhole formation in the Acque Albule basin of central Italy from geophysical and geochemical observations. Eng. Geol. 191, 36–47.

Barker, R., 1992. A simple algorithm for electrical imaging of the subsurface. First Break 10, 53–62.

Batayneh, A.T., Abueladas, A.A., Moumani, K.A., 2002. Use of ground-penetrating radar for assessment of potential sinkhole conditions: an example from Ghor al Haditha area, Jordan. Environ. Geol. 41, 977–983.

Beck, B.F. (Ed.), 2005. Sinkholes and the Engineering and Environmental Impacts of KarstGeotechnical Special Publication no. 144. American Society of Civil Engineers (677 pp.).

Bigi, S., Beaubien, S.E., Ciotoli, G., D'Ambrogi, C., Doglioni, C., Ferrante, V., Lombardi, S., Milli, S., Orlando, L., Ruggiero, L., Tartarello, M.C., Sacco, P., 2014. Mantle-derived CO_2 migration along active faults within an extensional basin margin (Fiumicino, Rome, Italy). Tectonophysics 637, 137–149.

Billi, A., Salvini, F., 2000. Sistemi di fratture associati a faglie in rocce carbonatiche: nuovi dati sull'evoluzione tettonica del Promontorio del Gargano. Boll. Soc. Geol. Ital. 119, 237–250.

Billi, A., Tiberti, M.M., 2009. Possible causes of arc development in the Apennines, central Italy. Geol. Soc. Am. Bull. 121, 1409–1420.

Billi, A., De Filippis, L., Ubertini, L., 2013. Acque e Travertini. Rend. Online Soc. Geol. Ital. 27 (109 pp.).

Billi, A., Doglioni, C., Nisio, S., 2014. Sinkhole a clessidra ed altri processi carsico-gravitativi nella Pianura Pontina: cantiere aperto e laboratorio naturale unico. In: Nisio, S. (Ed.), Voragini in Italia. ISPRA Istituto Superiore per la Protezione e Ricerca Ambientale, Rome, p. 8.

Billi, A., Tiberti, M.M., Cavinato, G.P., Cosentino, D., Di Luzio, E., Keller, J.V.A., Kluth, C., Orlando, L., Parotto, M., Praturlon, A., Romanelli, M., Storti, F., Wardell, N., 2006. First results from the CROP-11 deep seismic profile, central Apennines, Italy: evidence of mid-crustal folding. J. Geol. Soc. Lond. 163, 583–586.

Billi, A., Valle, A., Brilli, M., Faccenna, C., Funiciello, R., 2007. Fracture-controlled fluid circulation and dissolutional weathering in sinkhole-prone carbonate rocks from central Italy. J. Struct. Geol. 29, 385–395.

Bozzano, F., Esposito, C., Franchi, S., Mazzanti, P., Perissin, D., Rocca, A., Romano, E., 2015. Understanding the subsidence process of a Quaternary plain by combining geological and hydrogeological modeling with satellite InSAR data: the Acque Albule plain case study. Remote Sens. Environ. 168, 219–238.

Brinkmann, R., 2013. Florida Sinkholes: Science and Policy. University Press of Florida, Gainesville, Florida (256 pp.).

Brunetti, E., Jones, J.P., Petitta, M., Rudolph, D.L., 2013. Assessing the impact of large-scale dewatering on fault-controlled aquifer systems: a case study in the Acque Albule basin (Tivoli, central Italy). Hydrogeol. J. 21, 401–423.

Bruno, E., Calcaterra, D., Parise, M., 2008. Development and morphometry of sinkholes in coastal plains of Apulia, southern Italy. Preliminary sinkhole susceptibility assessment. Eng. Geol. 99, 198–209.

Buttrick, D., van Schalkwyk, A., 1998. Hazard and risk assessment for sinkhole formation on dolomite land in South Africa. Environ. Geol. 36, 170–178.

Capelli, G., Cosentino, D., Raffi, R., Ventura, G., 1987. Modalità di ricarica ed assetto strutturale dell'acquifero delle sorgenti Capore-S.Angelo (Monti Lucretili-Sabina meridionale). Geol. Romana 26, 419–447.

Caramanna, G., Ciotoli, G., Nisio, S., 2008. A review of natural sinkhole phenomena in Italian plain areas. Nat. Hazards 45, 145–172.

Carbonel, D., Rodríguez, V., Gutiérrez, F., Galve, J.P., Guerrero, J., Zarroca, M., Roqué, C., McCalpin, J.P., Acosta, E., 2014a. Investigating a damaging buried sinkhole cluster in an urban area (Zaragoza city, NE Spain) integrating multiple techniques: geomorphological surveys, DInSAR, DEMs, GPR, ERT, and trenching. Geomorphology 229, 3–16.

Carbonel, D., Rodríguez, V., Gutiérrez, F., McCalpin, J.P., Linares, R., Roqué, C., Zarroca, M., Guerrero, J., Sasowsky, I., 2014b. Evaluation of trenching, ground penetrating radar (GPR) and electrical resistivity tomography (ERT) for sinkhole characterization. Earth Surf. Process. Landf. 39, 214–227.

Carbonel, D., Gutiérrez, F., Linares, R., Roqué, C., Zarroca, M., McCalpin, J., Guerrero, J., Rodriguez, V., 2013. Differentiating between gravitational and tectonic faults by means of geomorphological mapping, trenching and geophysical surveys. The case of Zenzano Fault (Iberian Chain, N Spain). Geomorphology 189, 93–108.

Carucci, V., Petitta, M., Aravena, R., 2012. Interaction between shallow and deep aquifers in the Tivoli Plain (Central Italy) enhanced by groundwater extraction: a multi-isotope approach and geochemical modelling. Appl. Geochem. 27, 266–280.

Cavinato, G.P., DeCelles, P.G., 1999. Extensional basins in the tectonically bimodal central Apennines fold–thrust belt, Italy: response to corner flow above a subducting slab in retrograde motion. Geology 27, 955–958.

Centamore, E., Nisio, S., Rossi, D., 2009. The San Vittorino Sinkhole Plain: relationships between bedrock structure, sinking processes, seismic events and hydrothermal springs. Ital. J. Geosci. 128, 629–639.

Chiarabba, C., Amato, A., Anselmi, M., Baccheschi, P., Bianchi, I., Cattaneo, M., Cecere, G., Chiarluce, L., Ciaccio, M.G., De Gori, P., De Luca, G., Di Bona, M., Di Stefano, R., Faenza, L., Govoni, A., Improta, L., Lucente, F.P., Marchetti, A., Margheriti, L., Mele, L., Michelini, A., Monachessi, G., Moretti, M., Pastori, M., Piana, A.N., Piccinini, D., Roselli, D., Seccia, D., Valoroso, L., 2009. The 2009 L'Aquila earthquake: main shock and aftershocks. Geophys. Res. Lett. 36, 18. http://dx.doi.org/10.1029/2009GL039627.

Ciotoli, G., Di Loreto, E., Finoia, M.G., Liperi, L., Meloni, F., Nisio, S., Sericola, A., 2015. Sinkhole susceptibility, Lazio Region, central Italy. J. Maps http://dx.doi.org/10.1080/17445647.2015.1014939 (in press).

Ciotoli, G., Etiope, G., Florindo, F., Marra, F., Ruggiero, L., Sauer, P.E., 2013. Sudden deep gas eruption nearby Rome's airport of Fiumicino. Geophys. Res. Lett. 40, 5632–5636.

Cook, K.L., Van Nostrand, R.G., 1954. Interpretation of resistivity data over filled sinks. Geophys. Prospect. 21, 716–723.

De Filippis, L., Anzalone, E., Billi, A., Faccenna, C., Poncia, P.P., Sella, P., 2013a. The origin and growth of a recently-active fissure ridge travertine over a seismic fault, Tivoli, Italy. Geomorphology 195, 13–26.

De Filippis, L., Faccenna, C., Billi, A., Anzalone, E., Brilli, M., Soligo, M., Tuccimei, P., 2013b. Plateau versus fissure ridge travertines from Quaternary geothermal springs of Italy and Turkey: interactions and feedbacks among fluid discharge, paleoclimate, and tectonics. Earth Sci. Rev. 123, 35–52.

De Filippis, L., Rossetti, C., Billi, A., Faccenna, C., 2013c. Uomo, georisorse e faglie nel bacino delle Acque Albule, Italia centrale. Rend. Online Soc. Geol. Ital. 27, 86–97.

DeGroot-Hedlin, C., Constable, S., 1990. Occam's inversion to generate smooth, two-dimensional models form magneto telluric data. Geophysics 55, 1613–1624.

Del Bon, A., Sbarbati, C., Brunetti, E., Carucci, V., Lacchini, A., Marinelli, V., Petitta, M., 2015. Groundwater flow and geochemical modelling of the Acque Albule thermal basin (Central Italy): a conceptual model for evaluating influences of human exploitation on flowpath and thermal resource availability. Cent. Eur. Geol. 58, 152–170.

Di Salvo, C., Mazza, R., Capelli, G., 2013. Gli acquiferi in travertino del Lazio: schemi idrogeologici e caratteristiche chimico-fisiche. Rend. Online Soc. Geol. Ital. 27, 54–76.

Epting, J., Huggenberger, P., Glur, L., 2009. Integrated investigations of karst phenomena in urban environments. Eng. Geol. 109, 273–289.

Ezersky, M., 2008. Geoelectric structure of the Ein Gedi sinkhole occurrence site at the Dead Sea shore in Israel. J. Appl. Geophys. 64, 56–69.

Ezersky, M., Frumkin, A., 2013. Fault — dissolution front relations and the Dead Sea sinkhole problem. Geomorphology 201, 35–44.

Faccenna, C., Florindo, F., Funiciello, R., Lombardi, S., 1993. Tectonic setting and sinkholes features: case histories from western central Italy. Quat. Proc. 3, 47–57.

Faccenna, C., Funiciello, R., Montone, P., Parotto, M., Voltaggio, M., 1994. Late Pleistocene strike-slip tectonics in the Acque Albule Basin (Tivoli, Latium). Mem. Descrittive Carta Geol. Ital. 49, 37–50.

Faccenna, C., Soligo, M., Billi, A., De Filippis, L., Funiciello, R., Rossetti, C., Tuccimei, P., 2008. Late Pleistocene depositional cycles of the Lapis Tiburtinus travertine (Tivoli, Central Italy): possible influence of climate and fault activity. Glob. Planet. Chang. 63, 299–308.

Faulkner, T.L., 2009. The endokarstic erosion of marble in cold climates: corbel revisited. Prog. Phys. Geogr. 33, 805–814.

Floris, M., Bozzano, F., Strappaveccia, C., Baiocchi, V., Prestininzi, A., 2014. Qualitative and quantitative evaluation of the influence of anthropic pressure on subsidence in a sedimentary basin near Rome. Environ. Earth Sci. 72, 4223–4236.

Ford, D.C., 2006. Karst geomorphology, caves and cave deposits: a review of North American contributions during the past half century. In: Harmon, R.S., Wicks, C.M. (Eds.), Perspectives on Karst Geomorphology, Hydrology, and Geochemistry — A Tribute Volume to Derek C. Ford and William B. White. Geological Society of America Special Paper 404, pp. 1–14.

Ford, D.C., Williams, P., 1989. Karst Geomorphology and Hydrology. Unwin Hyman, London (562 pp.).

Frepoli, A.F., Marra, C., Maggi, A., Marchetti, A., Nardi, N., Pagliuca, M., Pirro, M., 2010. Seismicity, seismogenic structures, and crustal stress fields in the greater Rome area (central Italy). J. Geophys. Res. 115, B12303. http://dx.doi.org/10.1029/2009JB006322.

Frumkin, A., Ezersky, M., Al-Zoubi, A., Akkawi, E., Abueladas, A.R., 2011. The Dead Sea sinkhole hazard: geophysical assessment of salt dissolution and collapse. Geomorphology 134, 1102–1117.

Frumkin, A., Zaidner, Y., Naamana, Y., Tsatskin, A., Porat, N., Vulfsone, L., 2015. Sagging and collapse sinkholes over hypogenic hydrothermal karst in a carbonate terrain. Geomorphology 229, 45–57.

García-Moreno, I., Mateos, R.M., 2011. Sinkholes related to discontinuous pumping: susceptibility mapping based on geophysical studies. The case of Crestatx (Mallorca, Spain). Environ. Earth Sci. 64, 523–537.

Gasparini, C., Di Maro, R., Pagliuca, N., Pirro, M., Marchetti, A., 2002. Recent seismicity of the "Acque Albule" travertine basin. Ann. Geophys. 45, 537–550.

Gill, J.C., Malamud, B.D., 2014. Reviewing and visualizing the interactions of natural hazards. Rev. Geophys. 52, 680–722.

Gillieson, D., 1987. Tropical caves in retrospect and prospect. Prog. Phys. Geogr. 11, 511–532.

Guarino, P.M., Nisio, S., 2012. Anthropogenic sinkholes in the territory of the city of Naples (Southern Italy). Phys. Chem. Earth 49, 92–102.

Gulley, J.D., Martin, J.B., Moore, P.J., Murphy, J., 2013. Formation of phreatic caves in an eogenetic karst aquifer by CO_2 enrichment at lower water tables and subsequent flooding by sea level rise. Earth Surf. Process. Landf. 38, 1210–1224.

Gunn, J. (Ed.), 2004. Encyclopedia of Caves and Karst Science. Fitzroy Dearborn, New York & London (902 pp.).

Gutiérrez, F., Galve, J.P., Guerrero, J., Lucha, P., Cendrero, A., Remondo, J., Bonachea, J., Gutiérrez, M., Sánchez, J.A., 2007. The origin, typology, spatial distribution, and detrimental effects of the sinkholes developed in the alluvial evaporite karst of the Ebro River valley downstream Zaragoza city (NE Spain). Earth Surf. Process. Landf. 32, 912–928.

Gutiérrez, F., Galve, J.P., Lucha, P., Bonachea, J., Jordá, L., Jordá, R., 2009. Investigation of a large collapse sinkhole affecting a multi-storey building by means of geophysics and the trenching technique, Zaragoza city, NE Spain. Environ. Geol. 58, 1107–1122.

Gutiérrez, F., Parise, M., De Waele, J., Jourde, H., 2014. A review on natural and human-induced geohazards and impacts in karst. Earth-Sci. Rev. 138, 61–88.

Hao, Y., Wang, Y., Zhu, Y., Lin, Y., Wen, J.-C., Yeh, T.-C.J., 2009. Response of karst springs to climate change and anthropogenic activities: the Niangziguan Springs, China. Prog. Phys. Geogr. 33, 634–649.

Harley, G.L., Polk, J.S., North, L.A., Reeder, P.P., 2011. Application of a cave inventory system to stimulate development of management strategies: the case of west-central Florida, USA. J. Environ. Manag. 92, 2547–2557.

Heidari, M., Khanlari, G.R., Taleb Beydokhti, A.R., Momeni, A.A., 2011. The formation of cover collapse sinkholes in North of Hamedan, Iran. Geomorphology 132, 76–86.

Higuera-Diaz, I.C., Carpenter, P.J., Thompson, M.D., 2007. Identification of buried sinkholes using refraction tomography at Ft. Campbell army airfield, Kentucky. Environ. Geol. 53, 805–812.

Jennings, J.N., 1985. Karst Geomorphology. Basil Blackwell, Oxford (293 pp.).

Jung, C., Bobet, A., Asce, M., Siddiki, N.Z., Kim, D., 2011. Postconstruction evaluation of subgrades chemically treated with lime kiln dust. J. Mater. Civ. Eng. 23, 931–940.

Kaufmann, G., Romanov, D., 2009. Geophysical investigation of a sinkhole in the northern Harz foreland (North Germany). Environ. Geol. 59, 401–405.

Koutepov, V.M., 2008. Assessment of suffosion-related hazards in karst areas using GIS technology. Environ. Geol. 54, 957–962.

Krawczyk, C.M., Polom, U., Trabs, S., Dahm, T., 2012. Sinkholes in the city of Hamburg—new urban shear-wave reflection seismic system enables high-resolution imaging of subrosion structures. J. Appl. Geophys. 78, 133–143.

La Vigna, F., Carucci, V., Mariani, I., Minelli, L., Pascale, F., Mattei, M., Mazza, R., Tallini, M., 2012. Intermediate-field hydrogeological response induced by L'Aquila earthquake: the Acque Albule hydrothermal system (Central Italy). Ital. J. Geosci. 131, 475–485.

La Vigna, F., Mazza, R., Capelli, G., 2013a. Detecting the flow relationships between deep and shallow aquifers in an exploited groundwater system, using long-term monitoring data and quantitative hydrogeology: the Acque Albule basin case (Rome, Italy). Hydrol. Process. 27, 3159–3173.

La Vigna, F., Mazza, R., Capelli, G., 2013b. Le risorse idriche nei travertini della piana di Tivoli-Guidonia. La modellazione numerica come strumento di gestione degli acquiferi. Rend. Online Soc. Geol. Ital. 27, 77–85.

Loke, M.H., 1996. Manual for the RES2DINV. Advanced Geosciences Inc., Austin, Texas.

Loke, M.H., 1999. Electrical Imaging Surveys for Environmental and Engineering Studies, A Practical Guide to 2D and 3D Surveys. MALA Geoscience, Penang, Malaysia (www.abem.se).

Loke, M.H., Barker, R.D., 1996. Rapid least-square inversion of apparent resistivity pseudosections by a quasi-Newton method. Geophys. Prospect. 44, 131–152.

Lollino, P., Martimucci, V., Parise, M., 2013. Geological survey and numerical modeling of the potential failure mechanisms of underground caves. Geosyst. Eng. 16, 100–112.

Lunne, T., Robertson, P.K., Powell, J.J.M., 1997. Cone Penetration Testing in Geotechnical Practice. Blackie Academic, New York (352 pp.).

MacRobert, C.J., Kalumba, D., Beales, P., 2010. Penetration testing: test procedures and design use in South Africa. Civ. Eng. 18, 29–38.

MacRobert, C.J., Kalumba, D., Beales, P., 2011. Correlating standard penetration test and dynamic probe super heavy penetration resistance values in sandy soils. J. S. Afr. Inst. Civ. Eng. 53, 46–54.

Maiorani, A., Funiciello, R., Mattei, M., Turi, B., 1992. Stable isotope geochemistry and structural elements of the Sabina region (Central Apennines, Italy). Terra Nova 4, 484–488.

Manfra, L., Masi, U., Turi, B., 1976. La composizione isotopica dei travertini del Lazio. Geol. Romana 15, 127–174.

Margiotta, S., Negri, S., Parise, M., Valloni, R., 2012. Mapping the susceptibility to sinkholes in coastal areas, based on stratigraphy, geomorphology and geophysics. Nat. Hazards 62, 657–676.

Martínez-Moreno, F.J., Pedrera, A., Ruano, P., Galindo-Zaldívar, J., Martos-Rosillo, S., González-Castillo, L., Sánchez-Úbeda, J.P., Marín-Lechado, C., 2013. Combined microgravity, electrical

resistivity tomography and induced polarization to detect deeply buried caves: Algaidilla cave (Southern Spain). Eng. Geol. 162, 67–78.
Matthews, M.C., Clayton, C.R.I., Rigby-Jones, J., 2000. Locating dissolution features in the Chalk. Q. J. Eng. Geol. Hydrogeol. 33, 125–140.
Maxia, C., 1950. Il Bacino delle Acque Albule (Lazio). Contributi di Scienze Geologiche. Supplemento Ricerca Scientifica no. 27. Università di Roma La Sapienza, Rome.
Mendonca, A.F., Pires, A.C.B., Barros, J.G.C., 1993. Pseudo-sinkholes in lateritic terrains, Brasilia, Brazil. In: Beck, B.F. (Ed.), Applied Karst Geology. Balkema, Rotterdam, pp. 43–49.
Minissale, A., Kerrick, D.M., Magro, G., Murrell, M.T., Paladini, M., Rihs, S., Sturchio, N.C., Tassi, F., Vaselli, O., 2002. Geochemistry of Quaternary travertines in the region north of Rome (Italy): structural, hydrologic, and paleoclimatic implications. Earth Planet. Sci. Lett. 203, 709–728.
Nisio, S., 2008. Natural sinkhole phenomena in the Italian plain areas. Mem. Descrittive Carta Geol. Ital. 85 (482 pp.).
Nisio, S., Caramanna, G., Ciotoli, G., 2007. Sinkholes in Italy: first results on the inventory and analysis. Geol. Soc. Lond., Spec. Publ. 279, 23–45.
Patacca, E., Sartori, R., Scandone, P., 1992. Tyrrhenian basin and Apenninic arcs: kinematic relations since late Tortonian times. Mem. Soc. Geol. Ital. 45, 425–451.
Patterson, D.A., Davey, J.C., Cooper, A.H., Ferris, J.K., 1995. The investigation of dissolution subsidence incorporating microgravity geophysics at Ripon, Yorkshire. Q. J. Eng. Geol. Hydrogeol. 28, 83–103.
Pirro, M., Pagliuca, M.N., Capriotti, D., Nisio, S., Guarino, P.M., 2013. A sinkhole in the middle valley of the River Tiber: Vadimone lake. Mem. Descrittive Carta Geol. Ital. 93, 381–392.
Plastino, W., Panza, G.F., Doglioni, C., Frezzotti, M.L., Peccerillo, A., De Felice, P., Bella, F., Povinec, P.P., Nisi, S., Ioannucci, L., Aprili, P., Balata, M., Cozzella, M.L., Laubenstein, M., 2011. Uranium groundwater anomalies and active normal faulting. J. Radioanal. Nucl. Chem. 288, 101–107.
Plastino, W., Povinec, P.P., De Luca, G., Doglioni, C., Nisi, S., Ioannucci, L., Balata, M., Laubenstein, M., Bella, F., Coccia, E., 2010. Uranium groundwater anomalies and L'Aquila earthquake, 6th April 2009 (Italy). J. Environ. Radioact. 101, 45–50.
Poppe, S., Holohan, E.P., Pauwels, E., Cnudde, V., Kervyn, M., 2015. Sinkholes, pit craters, and small calderas: analog models of depletion induced collapse analyzed by computed X-ray microtomography. Geol. Soc. Am. Bull. 127, 281–296.
Pueyo-Anchuela, O., Casas-Sainz, A.M., Soriano, M.A., Pocoví-Juan, A., 2010. A geophysical survey routine for the detection of doline areas in the surroundings of Zaragoza NE Spain. Eng. Geol. 114, 382–396.
Ronchi, P., Cruciani, F., 2015. Continental carbonates as a hydrocarbon reservoir, an analog case study from the travertine of Saturnia, Italy. AAPG Bull. 99, 711–734.
Rossetti, F., Tecce, F., Billi, A., Brilli, M., 2007. Patterns of fluid flow in the contact aureole of the late Miocene Monte Capanne pluton (Elba Island, Italy): the role of structures and rheology. Contrib. Mineral. Petrol. 153, 743–760.
Salgado, R., Yoon, S., 2003. Dynamic cone penetration test (DCPT) for subgrade assessment. Report FHWA/IN/JTRP-2002/30Joint Transportation Research Program. Indiana Department of Transportation, Purdue University, West Lafayette, Indiana, USA.
Salvati, R., Sasowsky, I.D., 2002. Development of collapse sinkhole in areas of groundwater discharge. J. Hydrol. 264, 1–11.
Samyn, K., Mathieu, F., Bitri, A., Nachbaur, A., Closset, L., 2014. Integrated geophysical approach in assessing karst presence and sinkhole susceptibility along flood-protection dykes of the Loire River, Orléans, France. Eng. Geol. 183, 170–184.
Santo, A., Ascione, A., Del Prete, S., Di Crescenzo, G., Santangelo, N., 2011. Collapse sinkholes distribution in the carbonate massifs of central and southern Apennines. Acta Carsologica 40, 95–112.
Sargent, C., Goulty, N.R., 2009. Seismic reflection survey for the investigation of gypsum dissolution and subsidence at Hell Kettles, Darlington, UK. Q. J. Eng. Geol. Hydrogeol. 42, 31–38.
van Schoor, M., 2002. Detection of sinkholes using 2D electrical resistivity imaging. J. Appl. Geophys. 50, 393–399.
Schwartz, B.F., Schreiber, M.E., 2009. Quantifying potential recharge in mantled sinkholes using ERT. Ground Water 47, 370–381.
Sella, P., Billi, A., Mazzini, I., De Filippis, L., Pizzino, L., Sciarra, A., Quattrocchi, F., 2014. A newly-emerged (August 2013) artificially-triggered fumarole near the Fiumicino airport, Rome, Italy. J. Volcanol. Geotherm. Res. 280, 53–66.
Siart, C., Forbriger, M., Nowaczinski, E., Hecht, S., Höfle, B., 2013. Fusion of multi-resolution surface (terrestrial laser scanning) and subsurface geodata (ERT, SRT) for karst landform investigation and geomorphometric quantification. Earth Surf. Process. Landf. 38, 1135–1147.
Simón, J.L., Soriano, M.A., Pérez, A., Luzón, A., Pocoví, A., Gil, H., 2014. Interacting tectonic faulting, karst subsidence, diapirism and continental sedimentation in Pleistocene deposits of the central Ebro Basin (Spain). Geol. Mag. 151, 1115–1134.
Song, K.-I., Cho, G.-C., Chang, S.-B., 2012. Identification, remediation, and analysis of karst sinkholes in the longest railroad tunnel in South Korea. Eng. Geol. 135–136, 92–105.
Sowers, G.F., 1996. Building on Sinkholes: Design and Construction of Foundations in Karst Terrain. American Society of Civili Engineers, Danvers, Massachusetts, USA (202 pp.).
Stierman, D.J., 2004. Geophysical detection of caves and karstic voids. In: Gunn, J. (Ed.), Encyclopedia of Caves and Karst Science. Fitzroy Dearborn, New York, pp. 377–380.
Sudha, K., Israil, M., Mittal, S., Rai, J., 2009. Soil characterization using electrical resistivity tomography and geotechnical investigations. J. Appl. Geophys. 67, 74–79.
Tallini, M., Gasbarri, D., Ranalli, D., Scozzafava, M., 2006. Investigating epikarst using lowfrequency GPR: example from the Gran Sasso range Central Italy. Bull. Eng. Geol. Environ. 65, 435–443.
Terzaghi, K., Peck, R.B., Mesri, G., 1996. Soil Mechanics in Engineering Practice. third ed. John Wiley and Sons, New York.
Thierry, P., Debeblia, N., Bitri, A., 2005. Geophysical and geological characterization of karst hazards in urban environments: application to Orléans (France). Bull. Eng. Geol. Environ. 64, 139–150.
Tuckwell, G., Grossey, T., Owen, S., Stearns, P., 2008. The use of microgravimetry to detect small distributed voids and low-density ground. Q. J. Eng. Geol. Hydrogeol. 41, 371–380.
Valois, R., Camerlynck, C., Dhemaied, A., Guerin, R., Hovhannissian, G., Plagnes, V., Rejiba, F., Robain, H., 2011. Assessment of doline geometry using geophysics on the Quercy plateau karst (South France). Earth Surf. Process. Landf. 36, 1183–1192.
Vignaroli, G., Aldega, L., Balsamo, F., Billi, A., De Benedetti, A.A., De Filippis, L., Giordano, G., Rossetti, F., 2015. A way to hydrothermal paroxysm, Colli Albani Volcano, Italy. Geol. Soc. Am. Bull. 127, 672–687.
Waltham, A.C., Fookes, P.G., 2003. Engineering classification of karst ground conditions. Q. J. Eng. Geol. Hydrogeol. 36, 101–118.
Waltham, T., Bell, F., Culshaw, M., 2005. Sinkholes and Subsidence. Springer, Chichester (382 pp.).
Wiegand, C., Kringer, K., Geitner, C., Rutzinger, M., 2013. Regolith structure analysis — a contribution to understanding the local occurrence of shallow landslides (Austrian Tyrol). Geomorphology 183, 5–13.
Williams, P.W., 2004. Dolines. In: Gunn, J. (Ed.), Encyclopedia of Caves and Karst Science. Fitzroy Dearborn, New York, pp. 304–310.
Yechieli, Y., Abelson, M., Bein, A., Crouvi, O., Shtivelman, V., 2006. Sinkhole "swarms" along the Dead Sea coast: reflection of disturbance of lake and adjacent groundwater systems. Geol. Soc. Am. Bull. 118, 1075–1087.
Youssef, A.M., El-Kaliouby, H., Zabramawi, Y.A., 2012. Sinkhole detection using electrical resistivity tomography in Saudi Arabia. J. Geophys. Eng. 9, 655–663.
Zhou, W., Beck, B.F., 2008. Management and mitigation of sinkholes on karst lands: an overview of practical applications. Environ. Geol. 55, 837–851.
Zhou, W.F., Beck, B.F., Adams, A.L., 2002. Effective electrode array in mapping karst hazards with electrical resistivity tomography. Environ. Geol. 42, 922–928.
Zhou, W., Beck, B.F., Stephenson, J.B., 2000. Reliability of dipole–dipole electrical resistivity tomography for defining depth to bedrock in covered karst terranes. Environ. Geol. 39, 760–766.
Zohdy, A.R., 1989. A new method for the automatic interpretation of Schlumberger and Wenner sounding curves. Geophysics 54, 245–253.